Preprint no ...

Studies of the QED/EW corrections to $Z \to ll$ observables at the LHC

LHC EW working group

ABSTRACT

Draft as of: **October 17, 2019**.

Contents

1 Introduction

Content:
Short historical overview of LEP/Tevatron/early LHC.

1.1 Electroweak pseudo-observables at LEP

Authors: Fulvio, Elzbieta

The concept of electroweak pseudo-observables (EWPO) was essential in the final analysis of LEP1 data of [1]. The EWPO's at LEP were quantities like Z mass and width; the various $2 \to 2$ Z peak cross-sections, most of the $2 \to 2$ charge and spin asymmetries at the Z peak, plus the equivalent effective weak mixing angle, which is the main SM parameter under study in this article. They were derived directly from the experimental data in such a way that QED contributions and the kinematic cut-off effects were removed. The art of the Z line-shape and asymmetry analyses at LEP relied on the ability to reduce the many degrees of freedom from the experimental measurements to a sufficiently small set of intermediate variables, which could be precisely described by theory. With full one-loop accuracy in QED/EW theory (and even a bit beyond) this was prepared in the ZFITTER package [2, 3].

A theoretically sound separation of the QED/EW effects between the QED emissions and genuine virtual weak effects was essential for the phenomenology of LEP precision physics [1]. It was motivated by the structure of the amplitudes for single Z-boson production or (to a lesser degree) WW-pair production in e^+e^- collisions, as well as by the fact that QED bremsstrahlung occurs at a different energy scale than the electroweak processes. Even more importantly, with this approach, multi-loop calculations for the complete electroweak sector could be avoided. The QED terms were thus resummed in an exclusive exponentiation scheme implemented in Monte Carlo [4]. Note that these QED corrections modify the cross-section at the peak by as much as 40%. The details of this paradigm are explained for example in Ref. [5]. It was obtained as the result of a massive effort by the theory community, which will not be recalled in any detail here. From the practical phenomenology perspective, spin amplitudes are semi-factorised into a Born-like term(s) and functional factors responsible for bremsstrahlung [6].

A similar separation can also be achieved for dynamics of production process in pp collisions, which can be isolated from QED/EW corrections. It was explored recently in the case of configurations with high-p_T jets associated with the Drell-Yan production of Z [7] or W bosons [8] at the LHC. The potentially large electroweak Sudakov logarithmic corrections discussed in [9] represent yet another class of weak effects, separable from those discussed above and throughout this paper, and they are not discussed here because they are mainly relevant for dilepton masses beyond the range considered for the weak mixing angle measurement.

To assess precisely the size and impact of the so-called genuine weak corrections to the Born-like cross section for lepton pair production with a virtuality well below the threshold for WW pair production, the precision calculations and programs prepared for the LEP era: `KKMC` Monte Carlo [10] and `Dizet` electroweak (EW) library, were adapted to provide pre-tabulated EW corrections which could be used by LHC-specific programs like the `TauSpinner` package [11]. Currently, the `KKMC` Monte Carlo used is `Dizet` version `6.21` [12, 2]. Since the LEP times, the version of the `Dizet` library has been updated eg. [13, 14]. For the sake of compatibility, results from this version are shown as well, however the final numbers will be evaluated with the most recent versions of the program, the `Dizet` version `6.45` [15].

1.2 The weak mixing angle and effective weak mixing angle

Drafting some text here only

There are multiple approaches and conventions used to define the effective weak mixing angle(s), as illustrated e.g. in the Particle Data Group 2018 review [16]. This naming is therefore overloaded and may lead to confusion.

The fundamental quantity is the weak mixing angle, $\sin^2\theta_W$. In the on-shell convention and $\alpha(0)$ EW scheme, as discussed in more detail in Appendix **??**, the weak mixing angle is defined uniquely through the gauge-boson masses at tree level:

$$\sin^2\theta_W = s_W^2 = 1 - \frac{m_W^2}{m_Z^2}. \tag{1}$$

and this relation holds to all orders. If m_W is a derived input parameter calculated using higher-order corrections, the corresponding $\sin^2\theta_W$ gets updated. For example, in the $\alpha(0)$ v0 scheme at EW LO, the value of $\sin^2\theta_W$ =

Table 1: The theory predictions for on-shell and effective leptonic weak angle. Number from Particle Data Group 2018 review [16].

Weak angle	Notation	Value	Parametric uncertainty
On-shell weak angle	s_W^2	0.22343	$\pm$ 0.00007
Effective weak angle	$\sin^2\theta^{\ell}_{eff}$	0.23154	$\pm$ 0.00003

0.21215 (see Table 13). With EW NLO+HO corrections applied to calculate m_W, the value of $\sin^2\theta_W = 0.22352$ (see Table 19).

In the same EW $\alpha(0)$ v0 scheme there is also a clear definition of the observable $\sin^2\theta^f_{eff}(M_Z)$, which is called the effective weak mixing angle at the Z-pole, which is related to the ratio of the effective axial and vector couplings, g_Z^f (here we use "f" for quark or lepton):

$$g_Z^f = \frac{v_Z^f}{a_Z^f} = 1 - 4|q_f|(K_Z^f s_W^2 + I_f^2), \tag{2}$$

with

$$I_f^2 = \alpha^2(s)\frac{35}{18}[1 - \frac{8}{3}Re(K_Z^f)s_W^2], \tag{3}$$

and the flavour-dependent *effective weak mixing angles* as

$$\sin^2\theta^f_{eff} = Re(\mathscr{K}_Z^f)s_W^2 + I_f^2 \tag{4}$$

While the $\sin^2\theta_W$ generic for all flavours, and energy-scale not dependent, the $\sin^2\theta^f_{eff}$ is not. It is speciffically for a given flavour, and only at the Z-pole. In the name already is suggested as effective theory quantity, not necessarily the Standard Model gauge theory one. In Table 1 we quote the most updated numbers from Particle Data Group 2018 review [16].

Estimates for the total theoretical error from leading unknown higher order corrections on $\sin^2\theta^{\ell}_{eff}$ has been recently updated in [17]. The leading missing orders are three- and four-loop corrections, $O(\alpha^3)$, $O(\alpha\alpha_s^2)$ and $O(\alpha\alpha_s^3)$. The final estimate is $4.3\cdot 10^{-5}$, compatible with number quoted by final LEP publications [1] of $5.0\cdot 10^{-5}$. This is precision fully adequate for measurement at LHC.

While the measurement at LEP were done at different energies and then corrected with theoretical predictions to the values at Z-pole, at LHC it will be done differently. The measurements will be done in different mass and rapidity ranges, and then combined. At least it is present strategy. It is therefore of interest to extend the definition of $\sin^2\theta^f_{eff}$ outside the Z-pole region. This could be done in straightforward way

$$g^f_{eff}(s,t) = \frac{v^f_{eff}(s,t)}{a^f_{eff}(s,t)} = 1 - 4|q_f|(K^f(s,t)s_W^2 + I_f^2(s,t)) \tag{5}$$

where s,t stand for Mandelstam variables. and correspondingly

$$\sin^2\theta^f_{eff}(s,t) = Re(\mathscr{K}^f(s,t))s_W^2 + I_f^2(s,t) \tag{6}$$

The flavour dependent effective weak mixing angles, calculated using: Eq. (6), EW form-factors of `Dizet` library, and $\alpha(0)v0$ scheme, with on-shell $s_W^2 = 0.22352$ are shown on Fig. 1 as a function of the invariant mass of outgoing lepton pair and for $\cos\theta = 0.5$. In Table 2 we display value of effective weak missing angles averaged over specified mass windows.

Prepare in the $\sin^2\theta_{eff}$ *schemes, similar figure and table. Ask Fulvio et al.*

Table 2: The effective weak mixing angles $\sin^2\theta^f_{eff}$, for different mass windows and with/without box corrections. The form-factor corrections are averaged with realistic line-shape and $\cos\theta$ distribution.
Results from Dizet 6.21, should be updated to Dizet 6.45.

Parameter	$\sin^2\theta^\ell_{eff}$	$\sin^2\theta^{up-quark}_{eff}$	$\sin^2\theta^{down-quark}_{eff}$
	EW loops without box corrections		
$80 < m_{ee} < 100$ GeV	0.23171	0.23171	0.23146
$78 < m_{ee} < 82$ GeV	0.23179	0.23172	0.23159
$89 < m_{ee} < 93$ GeV	0.23170	0.23169	0.23147
$108 < m_{ee} < 112$ GeV	0.23168	0.23175	0.23137
	EW loops with box corrections		
$80 < m_{ee} < 100$ GeV	0.23171	0.23171	0.23146
$78 < m_{ee} < 82$ GeV	0.23136	0.23167	0.23158
$89 < m_{ee} < 93$ GeV	0.23168	0.23169	0.23147
$108 < m_{ee} < 112$ GeV	0.23246	0.23174	0.23130

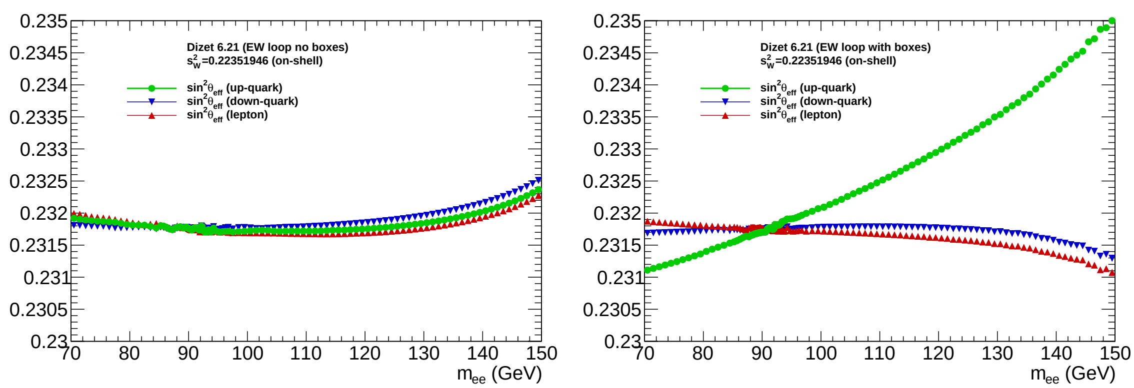

Figure 1: Effective weak mixing angles $\sin^2\theta^f_{eff}$ with EW corrections calculated using `Dizet` library and on-shell $s^2_W = 0.22352$ as a function of m_{ee} and $\cos\theta = 0$, without (left) and with (right) box corrections are shown.
Results from Dizet 6.21, should be updated to Dizet 6.45.

1.3 Observables sensitive to the weak mixing angle at hadron colliders

1.4 Interpretation of early hadron collider measurements in terms of the effective weak mixing angle

2 Virtual EW corrections

Authors: Elzbieta (Dizet), Fulvio (Powheg_ew), Serge/Lida (MCSANC), Doreen?(ZGRAD2)

Content:

- *Loops and box corrections with different EW schemes.*
- *Treatment of* $\alpha(M_Z)$ *with different EW schemes. Show numerical results.*
- *Treatment of* $\sin^2\theta_W$ *with different schemes. Show numerical results.*
- *Genuine EW and line-shape corrections to* $d\sigma/dm_{ll}$*,* A_{FB}*. Comparisons of* Powheg_ew*,* MCSANC *and* PowhegZj+wt^{EW}
- *Improved Born Approximation vs Effective Born. Comparisons from* PowhegZj+wt^{EW}.

2.1 Introduction

2.2 Overview of calculations/tools and input schemes

2.3 Numerical results for virtual EW corrections

2.3.1 Loops and box corrections with different EW schemes

In this Section we show comparison between Dizet and MCSANC EW libraries. For details on the calculations see respectively [12, 2] and [18, 19]. The input parameters, which could be set consistently in both programs, are collected in Table **??**.

The definition of the *effective* quark masses used in both initialisation and shown in Table **??** is such that they are some fitted values which allows to reproduce in the one-loop order the quantity of $\Delta\alpha_h^{(5)}(M_Z^2)$.

Comments:

For Dizet 6.21 *parametrisation of* α *not updated, used the one of published version. For measurements at LEP used probably updates of [20]. The comparison between* MCSANC *and* Dizet *should be updated to* Dizet 6.XX

Table 3: The EW parameters at EW NLO+HO, with on-mass-shell definition (LEP convention).

Parameter	$(\alpha(0), G_\mu, M_Z)$ $\alpha(0)$ v0	$(\alpha(0), M_W, M_Z)$ $\alpha(0)$ v1	(G_μ, M_Z, M_W) G_μ	$(\alpha(0), s_W^2, M_Z)$ $\sin^2_{eff}$ v1	(G_μ, s_W^2, M_Z) sin^2_{eff} v2
M_Z (GeV)	91.1876	91.1876	91.1876	91.1876	91.1876
$1/\alpha(M_Z)$	0.0077549256				
$\alpha(M_Z)$	128.9503020				
G_μ (GeV^{-2})	$1.1663787 \cdot 10^{-5}$		$1.1663787 \cdot 10^{-5}$		$1.1663787 \cdot 10^{-5}$
M_W (GeV)	80.358935	80.385	80.385		
s_W^2	0.223401084	0.22289722	0.22289722		
$\sin^2\theta^\ell_{eff}$	0.231499			0.231499	0.231499
$\sin^2\theta^u_{eff}$	0.231392				
$\sin^2\theta^d_{eff}$	0.231265				
$\sin^2\theta^b_{eff}$	0.232733				

2.3.2 α_{QED} with different EW schemes

2.3.3 $\sin^2\theta_W$ with different EW schemes

Table 4: The EW parameters used for: (i) the EW LO $\alpha(0)$ v0 scheme, (ii) effective Born spin amplitude around the Z-pole and (iii) effective Born with improved normalisation. In each case parameters are chosen that the SM relation, formula (8), is obeyed. The $G_\mu = 1.1663887 \cdot 10^{-5}$ GeV^{-2}, $M_Z = 91.1876$ GeV and $\mathcal{K}_f, \mathcal{K}_e, \mathcal{K}_{\ell f} = 1$.

EW LO $\alpha(0)$ scheme	Effective Born *LEP*	Effective Born *LEP with improved norm.*
$\alpha = 1/137.3599$ $s_W^2 = 0.21215$ $\rho_{\ell f} = 1.0$	$\alpha = 1/128.8667$ $s_W^2 = 0.23152$ $\rho_{\ell f} = 1.0$	$\alpha = 1/128.8667$ $s_W^2 = 0.23152$ $\rho_{\ell f} = 1.005$

2.3.4 Improved Born Approximation and Effective Born

Comment: Content of this subsection was published in [21].

The *Improved Born Approximation* (IBA) is discussed in more details in Appendix B. In IBA, the complete $O(\alpha)$ EW corrections, supplemented by selected higher order terms, are handled with form-factor corrections, dependent on (s,t), multiplying couplings and propagators of the usual Born expressions.

At this point we would like to introduce two options for the Born spin amplitudes *parametrisation*, which we will refer to as *Effective Born*, which work as very good approximations of the EW corrections near the Z-pole. We denote them respectively as *LEP* and *LEP with improved norm.*. The *Effective Born* absorbs bulk of EW corrections into redefinition of few fixed parameters (couplings) instead.

- The *LEP* parametrisation is using formula (26) for spin amplitude but with $\alpha(s) = \alpha(M_Z) = 1./128.8667$, $s_W^2 = \sin^2\theta_W^{eff}(M_Z) = 0.23152$ and all form factors equal to 1.0. The values are as measured at the Z-pole and reported in [22].
- The *LEP with improved norm.* parametrisation is using formula (26) for spin amplitude, parameters are set as for *LEP* parametrisation, and all form-factors equal 1, except $\rho_{\ell f} = 1.005$. This again correspond to the measured value $\rho(M_Z) = 1.005$ also reported in [22].

Table 4 shows (i) effective Born (*LEP*) parametrisation and (ii) effective Born (*LEP with improved norm.*). In each case parameters are chosen that the SM relation, formula (8), is obeyed.

In the following, we will systematically compare predictions of EW corrections and those calculated with *LEP* or *LEP with improved norm.* approximations. As we will see later, effective Born with *LEP with improved norm.* works well around Z-pole both for predicting the lineshape and forward-backward asymmetry.

2.3.5 The Z-boson lineshape

In the EW LO, the Z-boson lineshape, assuming that the constraint (38) holds, depends only on two parameters (M_Z, Γ_z). The effect on the lineshape from EW loop corrections are due to corrections to the propagators: vacuum polarisation corrections (running α) and ρ form-factor, causing change in relative contributions of the Z and γ, and change of the Z-boson vector to axial coupling ratio ($\sin^2\theta_{eff}$). The above affect not only shape but also normalisation of the cross-section.

In Fig. 2 (top-left) distributions of generated and EW corrected lineshape are shown. On the logarithmic scale difference is barely visible. In the following plots of the same Figure we study it in more details. The ratios of the lineshape distributions with gradually introduced EW corrections are shown. For reference ones (denominator) the following: (i) EW LO $\alpha(0)$, (ii) effective Born *(LEP)* and (iii) effective Born *(LEP with improved norm.)* are used. At the Z-pole, complete EW corrections are at about 0.1% for the one with effective Born *(LEP with improved norm.)*. It shows that using for events generation EW LO matrix element but with different parametrisations will significantly reduce the size of missing EW corrections.

Table 5: EW corrections to cross-sections in the specified mass windows. The EW weight is calculated with $\cos\theta^*$ definition for scattering angle.

Corrections to cross-section	$89 < m_{ee} < 93$ GeV	$80 < m_{ee} < 100$ GeV
σ(EW corr. to m_W)/σ(EW LO $\alpha(0)$)	0.97114	0.97162
σ(EW corr. to $\chi(Z),\chi(\gamma)$)/σ(EW LO $\alpha(0)$)	0.98246	0.98346
σ(EW/QCD FF no boxes)/σ(EW LO $\alpha(0)$)	0.96469	0.96602
σ(EW/QCD FF with boxes)/σ(EW LO $\alpha(0)$)	0.96473	0.96607
σ(*LEP*)/σ(EW/QCD FF with boxes)	1.01102	1.01093
σ(*LEP with improved norm.*)/σ(EW/QCD FF with boxes)	1.00100	1.00098

Table 6: The difference in forward-backward asymmetry, ΔA_{FB}, in the specified mass windows. The difference is calculated using $\cos\theta^{CS}$ to define forward and backward hemisphere. The EW weight is calculated with $\cos\theta^*$ definition for scattering angle.
Numbers should be updated with Dizet 6.XX form factors.

Corrections to A_{FB}	$89 < m_{ee} < 93$ GeV	$80 < m_{ee} < 100$ GeV
A_{FB}(EW corr. m_W) - A_{FB}(EW LO $\alpha(0)$)	-0.02097	-0.02103
A_{FB}(EW corr. prop. $\chi(Z),\chi(\gamma)$) - A_{FB}(EW LO $\alpha(0)$)	-0.02066	-0.02098
A_{FB}(EW/QCD FF no boxes) - A_{FB}(EW LO $\alpha(0)$)	-0.03535	-0.03569
A_{FB}(EW/QCD FF with boxes) - A_{FB}(EW LO $\alpha(0)$)	-0.03534	-0.03567
A_{FB}(*LEP*) - A_{FB}(EW/QCD FF with boxes)	-0.00006	-0.00001
A_{FB}(*LEP with improved norm.*) - A_{FB}(EW/QCD FF with boxes)	-0.00005	-0.00002

Table 5 details numerical values for EW corrections to the normalisation (ratios of the cross-section), integrated in the range $80 < m_{ee} < 100$ GeV and $89 < m_{ee} < 93$ GeV. Results from calculating EW weight using $\cos\theta^*$ definition of the scattering angle are shown. Total EW correction to normalisation at EW LO G_μ is 1.010. Total EW correction to normalisation at EW LO $\alpha(0)$ is about 0.965, while total corrections to the effective Born *(LEP with improved norm.)* is of about 1.001.

2.3.6 The A_{FB} distribution

The forward-backward asymmetry defined for pp collisions in a standard way reads

$$A_{FB} = \frac{\sigma(\cos\theta > 0) - \sigma(\cos\theta < 0)}{\sigma(\cos\theta > 0) + \sigma(\cos\theta < 0)}, \tag{7}$$

where $\cos\theta$ is taken in the *Collins-Soper* frame.

The EW corrections change overall normalisation and the shape of A_{FB}, particularly around the Z-pole. In Fig. 3 (top-left), the A_{FB} distribution as generated (EW LO) and EW corrected are shown. In the following plots of this Figure, we study it in more details. The difference $\Delta A_{FB} = A_{FB} - A_{FB}^{ref}$ with gradually introduced EW corrections are shown. For reference the following ones: (i) EW LO $\alpha(0)$, (ii) effective Born *(LEP)* and (iii) effective Born *(LEP with improved norm.)* are used.

Complete EW corrections to A_{FB} integrated around Z-pole, are about ΔA_{FB} = -0.00075 with respect to EW LO G_μ predictions and about ΔA_{FB} = -0.03534 with respect to EW LO with $\alpha(0)$ predictions. The total corrections to A_{FB} of effective Born (*LEP with improved norm.*) is ΔA_{FB} = -0.00005. Using effective Born *(LEP improved norm.)* configuration reproduces EW loop corrections predictions with precision better than ΔA_{FB} = -0.0001 in the full mass range shown, but the remaining box corrections are at ΔA_{FB} = -0.002 around $m_{ee} = 150$ GeV.

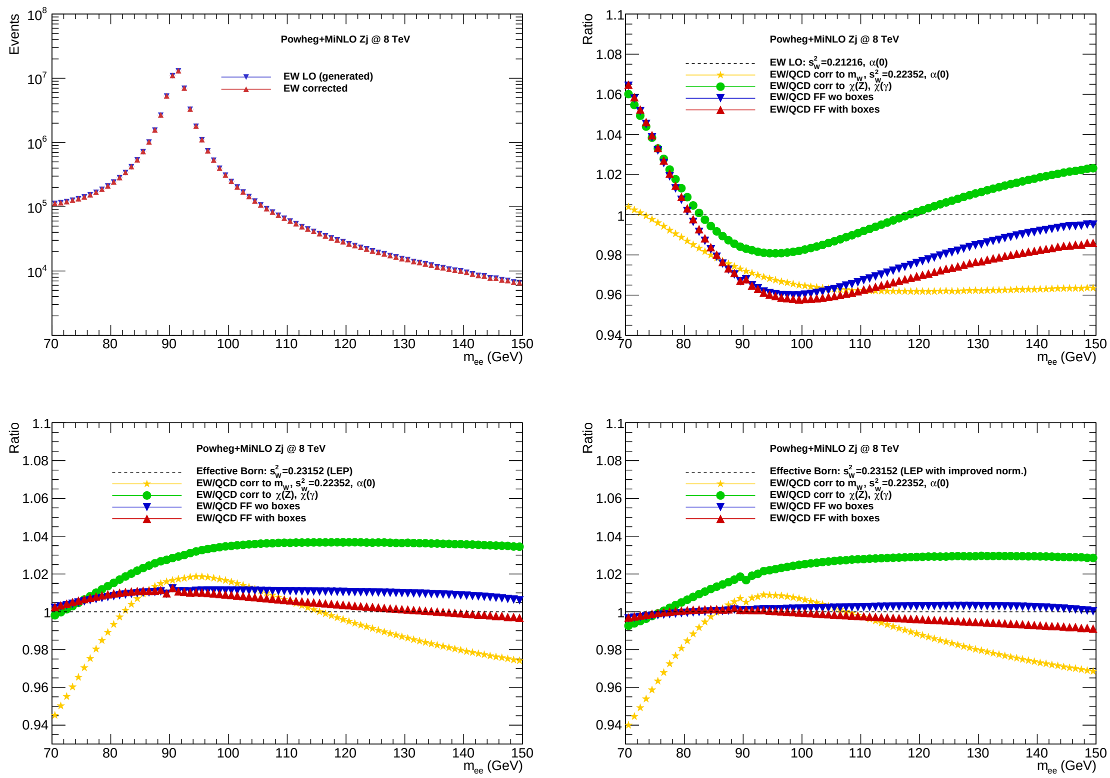

Figure 2: Top-left: lineshape distribution as generated with `Powheg+MiNLO` (blue triangles) and after reweighting introducing all EW corrections discussed (red triangles). The points are barely distinguishable. Ratios of the lineshapes with gradually introduced EW corrections. In consecutive plots as a reference (black dashed line): (i) reweighted to EW LO $\alpha(0)$ scheme (top-right), (ii) reweighted to effective Born *(LEP)* (bottom-left) and (iii) reweighted to effective Born *(LEP with improved norm.)* (bottom-right) was used.

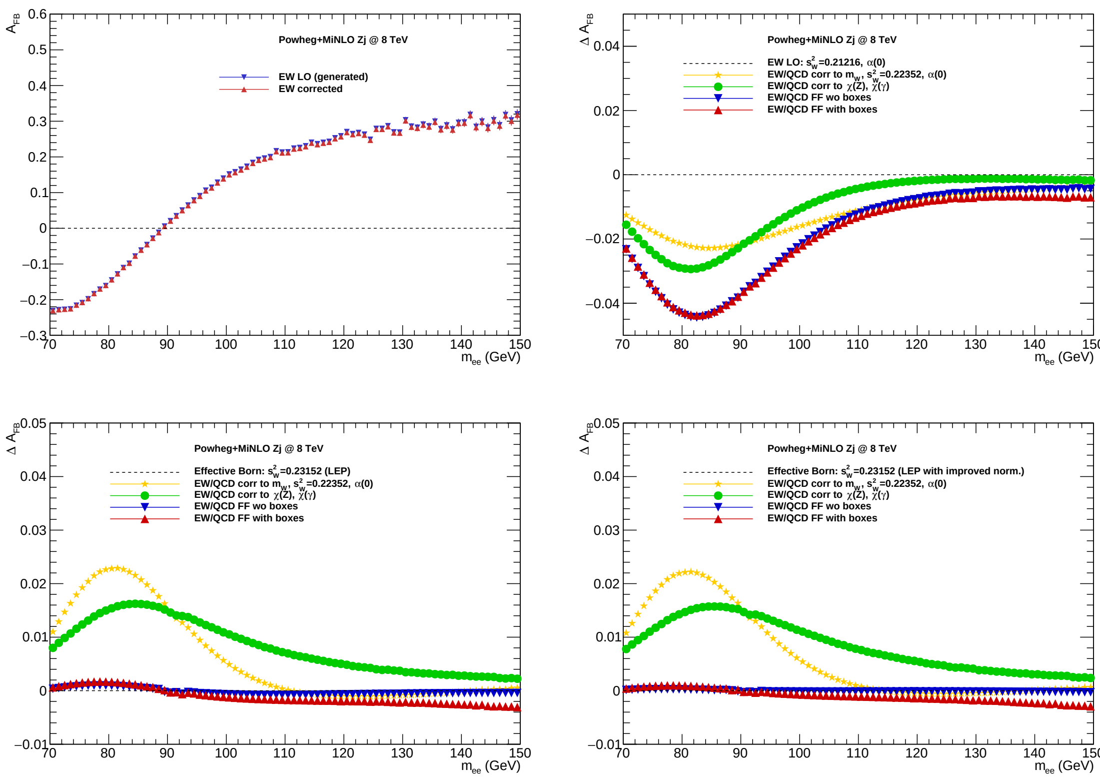

Figure 3: Top-left: the A_{FB} distribution as generated in `Powheg+MiNLO` sample (blue triangles) and after reweighting introducing all EW corrections (red triangles). The two choices are barely distinguishable.The differences $\Delta A_{FB} = A_{FB} - A_{FB}^{ref}$, due to gradually introduced EW corrections. In consecutive plots as a reference (black dashed line): (i) reweighted to EW LO $\alpha(0)$ scheme (top-right), (ii) reweighted to effective Born *(LEP)* (bottom-left) and (iii) reweighted to effective Born *(LEP with improved norm.)* (bottom-right) was used.
Plots should be updated with Dizet 6.XX form factors.

Table 7: Shown availability for QCD corrections and EW schemes with different codes.

Program	QCD	EW	EW scheme	Comments
Powheg_ew	LO	LO	$\alpha(0)$ v0	pole mass, fixed Γ_Z
		LO, NLO, NLO+HO	$\alpha(0)$ v1	
		LO, NLO, NLO+HO	G_μ	
		LO, NLO, NLO+HO	$\sin^2\theta_{eff}$ v1	
		LO, NLO, NLO+HO	$\sin^2\theta_{eff}$ v2	
	NLO	NLO+HO	G_μ	pole mass, fixed Γ_Z
MCSANC	LO	LO, NLO, NLO+HO	$\alpha(0)$ v1	pole mass, fixed Γ_Z
		LO, NLO, NLO+HO	G_μ	
Dizet FF+wt^{EW}	MC event	LO, NLO+HO	$\alpha(0)$ v0	on-shell mass, running Γ_Z[1]

2.4 Benchmark results from Powheg_ew, MCSANC, PowhegZj+wt^{EW}

In this section we collect results for Powheg_ew, MCSANC and PowhegZj+wt^{EW}, for benchmark EW schemes defined as in Table 13. Not all EW schemes where implemented in all programs. Table 7 specify the order of QCD and EW corrections which were used for the comparisons presented in this Section.

Comparisons between different programs and EW calculations are performed for the ratios of differential cross-sections and the differences of forward-backward asymmetries, between EW LO and NLO or NLO+HO predictions, always calculated with the same program. Those ratios or differences are then compared between different calculations. This approach to large extend minimises impact from not *tuned* QCD component of the predictions: structure functions, QCD scale, matrix element order, etc. Also, as pointed in Table 7, two out of three programs are using pole mass and fixed Γ_Z, while the third one is using on-shell mass and running Γ_Z.

The PowhegZj+wt^{EW} which is using form-factors from Dizet library, also provides predictions for the (NLO+HO - LO) corrections in other schemes. The wt^{EW}, as exlained in Appendix E is used to are reweighted at EW LO to different schemes. Then it is assumed that absolute predictions in different EW schemes should agree at NLO+HO, which indeed is the case for Powheg_ew estimates, see Tables 26 and 27. With this assumptions, the ratios NLO+HO/LO or differences NLO+HO - LO can be calculated with PowhegZj+wt^{EW}, using predictions of EW NLO+HO with $\alpha(0)$ v0 scheme and EW LO with either of three schemes.

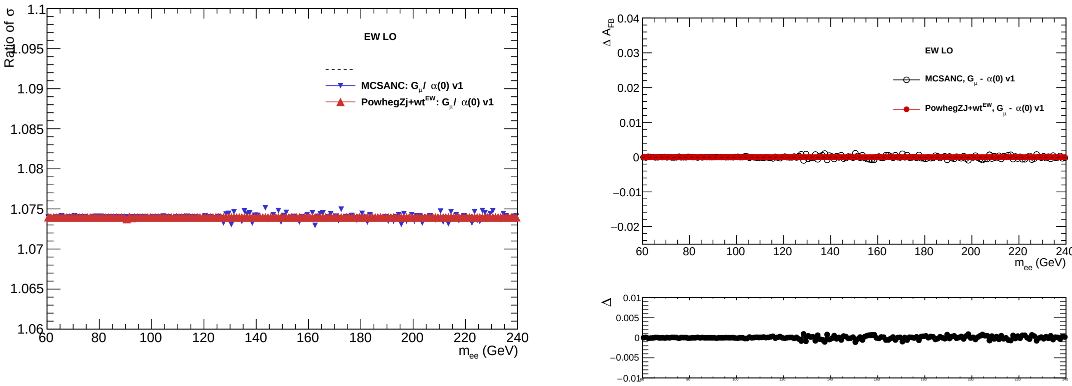

Figure 4: The EW LO predictions for radio of cross-sections and ΔA_{FB} between different EW schemes: $\alpha(0)$ v0 and G_μ. Shown results with `PowhegZj + ` wt^{EW} and `MCSANC`.
Make better quality plot

2.4.1 Benchmarks at EW LO

Comparison of the cross-sections ratios for different EW schemes, predicted by `Powheg_ew` and `PowhegZj`+wt^{EW} are shown in Table 8. Similar comparison for forward-backward asymmetry is shown in Table 9. The ratio of line-shapes and difference for forward-backward asymmetry are shown in Fig. 4. comparison between `MCSANC` and `PowhegZj`+wt^{EW}. Similar agreement was obtained when comparing with `Powheg_ew`. They confirm very good tuning at EW LO and also that comparisons between programs with different implementation of QCD components can be done quite precisely, ones comparing ratios or differences of ratios. For `Powheg_ew` shown are also absolute predictions, while for `PowhegZj`+wt^{EW} are not[2]. Note for example that as at EW LO, schemes $\alpha(0)$ v1 and G_μ were tuned to share the same value of s_W^2, the difference $A_{FB}(G_\mu)$ - $A_{FB}(\alpha(0)$ v1) is equal to zero,

[2]The reason is that `PowhegZj` events were generated with somewhat arbitrary setting for QCD and EW parts (e.g. $sin^2\theta_W$=0.23113, fixed Γ_Z in the propagator, on-shell Z mass), so obtained results should not be quoted as the reference ones. They are however reweighted to EW $\alpha(0)$ v0 scheme before any benchmarks are evaluated.

Table 8: Cross-sections and cross-section ratios estimated at EW LO with Powheg_ew and PowhegZj+wt^{EW}, for three mass windows.

	m_{ee} = 89 - 93 GeV	m_{ee} = 80 - 100 GeV	m_{ee} = 70 - 120 GeV
Cross-section [pb]			
Powheg_ew			
$\alpha(0)$ v0	630.848722	906.156051	959.658977
$\alpha(0)$ v1	571.411296	821.363274	870.729908
G_μ	612.514433	880.446121	933.363827
Cross-section ratios			
$\alpha(0)$ v1/ $\alpha(0)$ v0			
Powheg_ew	0.905782	0.906426	0.907333
PowhegZj+wt^{EW}	0.905596	0.906462	0.907347
G_μ / $\alpha(0)$ v0			
Powheg_ew	0.970937	0.971627	0.972600
PowhegZj+wt^{EW}	0.972622	0.973550	0.974501
G_μ / $\alpha(0)$ v1			
Powheg_ew	1.071933	1.071933	1.071933
PowhegZj+wt^{EW}	1.074010	1.074010	1.074010

Table 9: Cross-sections difference in forward and backward hemispheres and forward-backward asymmetry as estimated at EW LO with Powheg_ew and PowhegZj+wt^{EW}, for three mass windows. The pole definition is used for input parameters as in Table 14.

	m_{ee} = 89 - 93 GeV	m_{ee} = 80 - 100 GeV	m_{ee} = 70 - 120 GeV
Forward-backward asymmetry A_{FB}			
Powheg_ew			
$\alpha(0)$ v0	0.06691361	0.06392369	0.06253754
$\alpha(0)$ v1	0.04653886	0.04343789	0.04212883
G_μ	0.04653886	0.04343789	0.04212883
ΔA_{FB}			
$\alpha(0)$ v1 - $\alpha(0)$ v0			
Powheg_ew	0.020375	0.020486	0.020487
PowhegZj+wt^{EW}	0.019800	0.020040	0.019978
G_μ - $\alpha(0)$ v0			
Powheg_ew	0.020375	0.020486	0.020487
PowhegZj+wt^{EW}	0.019800	0.020040	0.019978
G_μ - $\alpha(0)$ v1			
Powheg_ew	0.0	0.0	0.0
PowhegZj+wt^{EW}	0.0	0.0	0.0

2.4.2 Benchmarks at EW NLO, NLO+HO

The following tables and figures contain comparisons between ratio of cross-sections or differences of forward-backward asymmetries between different EW schemes or same EW scheme but different level of corrections.

Tables:

- Table 10: Cross-sections ratios estimated with `Powheg_ew` and `PowhegZj`+wt^{EW}, different EW schemes, comparison at EW LO and NLO+HO.
- Table 11: Forward-backward asymmetry differences as estimated by `PowhegZj`+wt^{EW} and `Powheg_ew`, different EW schemes, comparison at EW LO and NLO+HO.

Figures:

- Figure 5: The lineshape predictions with `Powheg_ew` and `MCSANC`. Comparison of ratios EW NLO/LO and NLO+HO/LO.
- Figure 6: The lineshape predictions with `Powheg_ew`, `MCSANC` and `PowhegZj`+wt^{EW}. Comparison of EW NLO+HO/LO, different EW schemes.
- Figure 7: The ΔA_{FB} predictions with `Powheg_ew` and `MCSANC`. Comparison at EW LO, NLO, NLO+HO, different EW schemes.
- Figure 8: The ΔA_{FB} predictions with `Powheg_ew` and `MCSANC` and `PowhegZj`+wt^{EW}. Comparisons of EW LO, NLO, NLO+HO, different EW schemes.

Observations:

- Tables 10 and 11 shows very good agreement between `Powheg_ew` and `PowhegZj`+wt^{EW} predictions for cross-section NLO+HO/LO and A_{FB} NLO+HO -HO corrections in $\alpha(0)$ v1 and G_μ schemes.
- Figure 5:
  Top plots: Very good agreement between `MCSANC` and `Powheg_ew` for σ_{NLO}/σ_{LO}. Both EW schemes: $\alpha(0)$ v1 and G_μ.
  Bottom plots: Apparent shift in $\sigma_{NLO+HO}/\Delta\sigma_{LO}$ for $\alpha(0)$ v1 scheme. Almost OK for G_μ scheme.
- Figure 6:
  Top plots: same observation as above about disagreement on HO corrections between `MCSANC` and `Powheg_ew` for $\alpha(0)$ v1 scheme.
  Bottom plot: `PowhegZj`+wt^{EW} and `Powheg_ew` in good agreement for NLO+HO at Z-pole, but discrepant at the level on 0.005 in relative corrections below and above Z peak.
- Figure 7:
  Top plots: Very good agreement between `MCSANC` and `Powheg_ew` for $\Delta A_{FB}(NLO-LO)$. Both EW schemes: $\alpha(0)$ v1 and G_μ.
  Bottom plots: Apparent shift in $\Delta A_{FB}(NLO+HO-LO)$ for $\alpha(0)$ v1 scheme. Almost OK for G_μ scheme.
- Figure 8:
  Top plots: same observation as above about disagreement on HO corrections between `MCSANC` and `Powheg_ew` for $\alpha(0)$ v1 scheme.
  Bottom plot: `PowhegZj`+wt^{EW} and `Powheg_ew` in good agreement for NLO+HO at Z-pole and below, but discrepant at the level up to 0.005 in absolute corrections above Z peak.

2.5 Theoretical uncertainties and conclusions

Table 10: Cross-sections ratios estimated with `Powheg_ew` and `PowhegZj`+wt^{EW} for three mass windows.

	EW order	m_{ee} = 89 - 93 GeV	m_{ee} = 80 - 100 GeV	m_{ee} = 70 - 120 GeV
`Powheg_ew`	NLO+HO/LO			
$\alpha(0)$ v1		1.06325	1.06374	1.06435
G_μ		0.99104	0.99229	0.99284
`MCSANC`	NLO+HO/LO			
$\alpha(0)$ v1		1.051194	1.066182	1.066778
G_μ		0.992299	0.992740	0.993295
`PowhegZj`+wt^{EW}	NLO+HO/LO			
$\alpha(0)$ v0		0.96452	0.96611	0.96757
$\alpha(0)$ v1		1.06506	1.06580	1.06640
G_μ		0.99167	0.99223	0.99289

Table 11: Forward-backward asymmetry differences as estimated by `PowhegZj`+wt^{EW} and `Powheg_ew`, for three mass windows.

ΔA_{FB}	EW order	m_{ee} = 89 - 93 GeV	m_{ee} = 80 - 100 GeV	m_{ee} = 70 - 120 GeV
`Powheg_ew`	NLO+HO - LO			
$\alpha(0)$ v1		-0.015706	-0.015733	-0.015632
G_μ		-0.015636	-0.015660	-0.015560
`MCSANC`	NLO+HO - LO			
$\alpha(0)$ v1		-0.001444	-0.001444	-0.001436
G_μ		-0.001523	-0.001525	-0.001516
`PowhegZj`+wt^{EW}	NLO+HO - LO			
$\alpha(0)$ v1		-0.015838	-0.015792	-0.015688
G_μ)		-0.015838	-0.015792	-0.015688

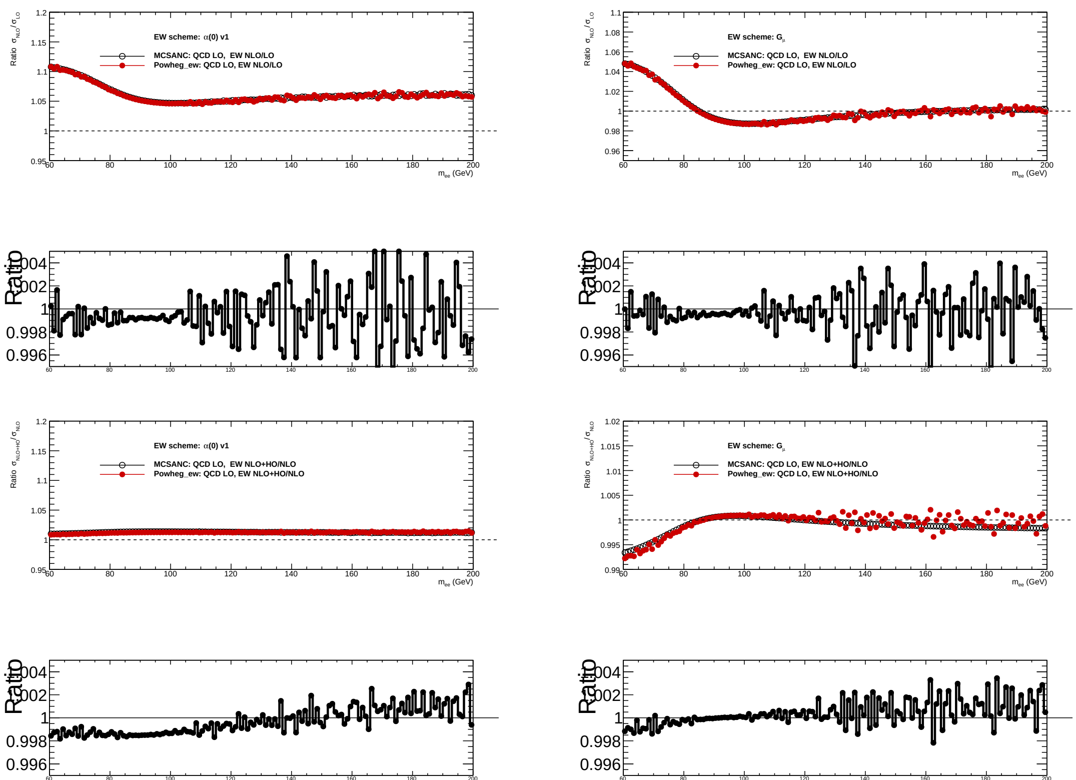

Figure 5: The lineshape predictions with `Powheg_ew`, `MCSANC`. Comparison of EW NLO/LO and NLO+HO/NLO.

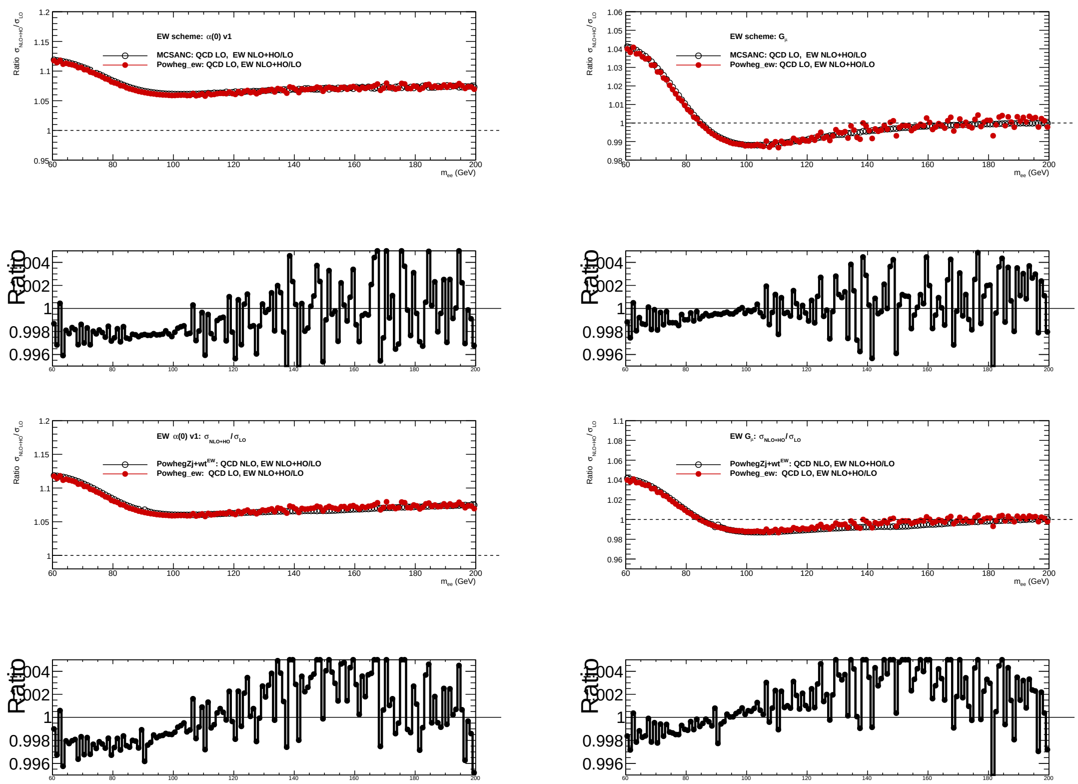

Figure 6: The lineshape predictions with Powheg_ew, MCSANC and PowhegZj+wt^{EW}. Comparisons of EW NLO+HO/LO, different EW schemes.

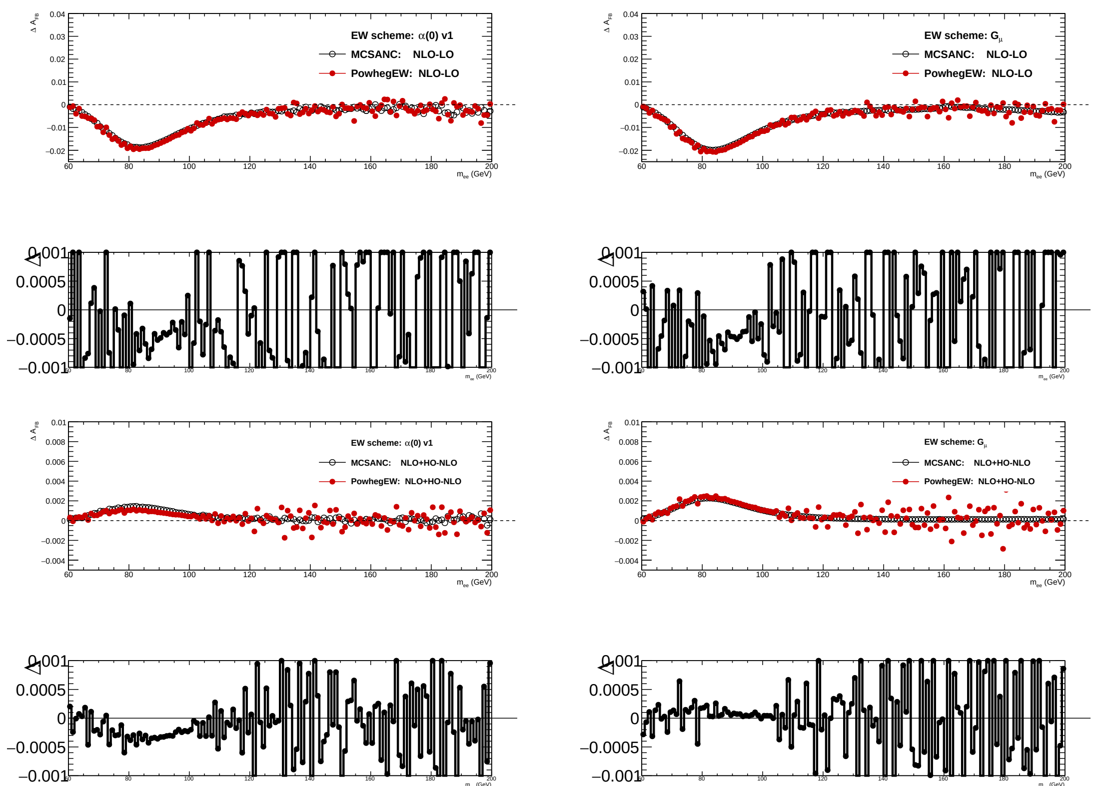

Figure 7: The ΔA_{FB} predictions with Powheg_ew and MCSANC. Comparisons of EW LO, NLO, NLO+HO, different EW schemes.

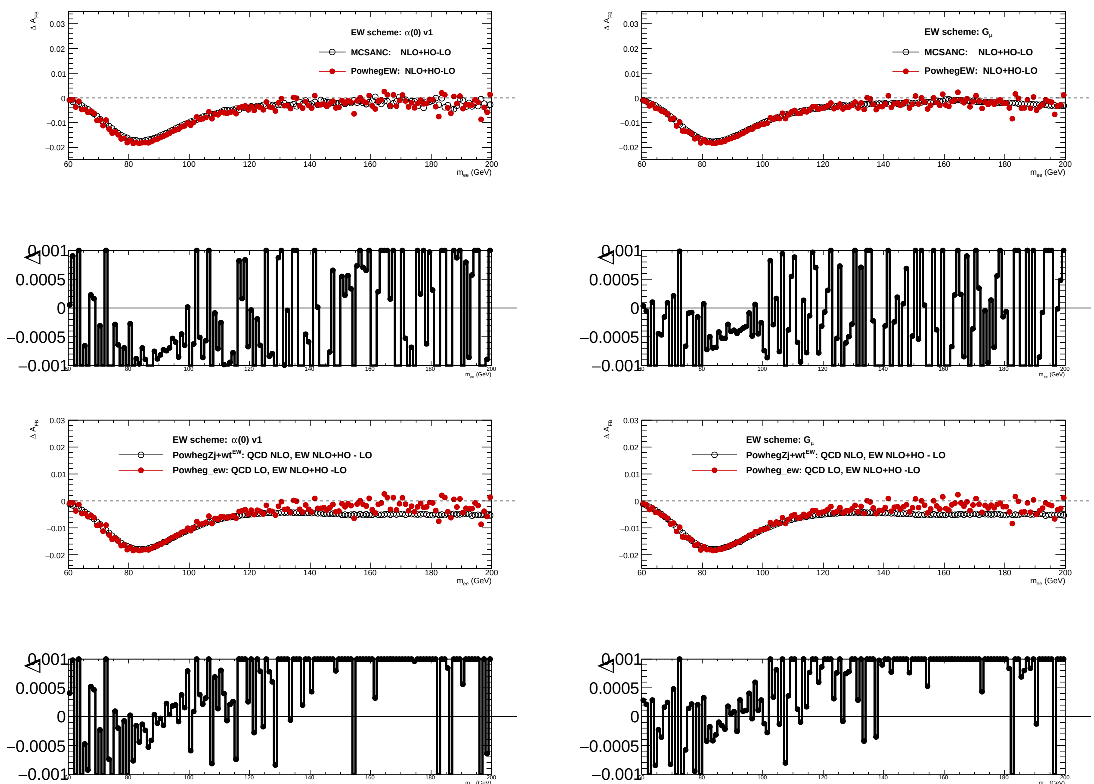

Figure 8: The ΔA_{FB} predictions with `Powheg_ew`, `MCSANC` and `PowhegZj`+wt^{EW}. Comparisons of EW LO, NLO+HO, different EW schemes.

3 QED emissions

Authors: Alessandro (`HORACE`), Fulvio (`Powheg_ew`), Serge/Lida (`MCSANC`), Scott (`KKMC-hh`), Doreen?(`ZGRAD2`)

Content:

- *Separation of contributions from ISR and IFI.*
- *Photon-induced processes and use of LUXQED PDFs*
- *Short description of calculations and tools used and of their configuration*
- *Numerical results and comparisons*
- *Theoretical uncertainties and conclusions*

3.1 Introduction

3.2 Overview of calculations and tools

3.3 Numerical results for QED ISR and IFI

3.4 Photon-induced processes

3.5 Theoretical uncertainties and conclusions

4 A possible strategy for run-2 measurements and combinations at the LHC

Authors: ATLAS/CMS/LHCb/theorists

Content:

- *Differential observables and expected measurement uncertainties*
- *Intepretation tools*
- *Combination tools*
- *Expected uncertainties and conclusions*

4.1 Introduction

4.2 Observables used for comparisons of expectations between experiments

4.3 Interpretation tools

4.3.1 QCD tools: `DYTurbo, NNLOJET`

4.3.2 QED/EW tools: `Dizet, Powheg EW, MC-SANC, ZGRAD2?`

4.4 Combination tools

4.4.1 Correlations between measurements: PDFs, QCD, QED/EW

4.4.2 Profile likelihood fit to all observables and direct extraction of weak mixing angle

4.4.3 Compatibility tests between measurements of different experiments

4.4.4 Profile likelihood fit to all observables and direct extraction of weak mixing angle

4.5 Expected breakdown of uncertainties and conclusions

4.5.1 Measurement uncertainties

4.5.2 PDF uncertainties

4.5.3 QED/EW uncertainties

4.5.4 QCD uncertainties

4.5.5 Parametric uncertainties

4.5.6 Conclusions

Acknowledgments

References

[1] SLD Electroweak Group, DELPHI, ALEPH, SLD, SLD Heavy Flavour Group, OPAL, LEP Electroweak Working Group, L3 Collaboration, S. Schael *et al.*, *Phys. Rept.* **427** (2006) 257–454, hep-ex/0509008.

[2] D. Yu. Bardin, P. Christova, M. Jack, L. Kalinovskaya, A. Olchevski, S. Riemann, and T. Riemann, *Comput. Phys. Commun.* **133** (2001) 229–395, hep-ph/9908433.

[3] A. B. Arbuzov, M. Awramik, M. Czakon, A. Freitas, M. W. Grunewald, K. Monig, S. Riemann, and T. Riemann, *Comput. Phys. Commun.* **174** (2006) 728–758, hep-ph/0507146.

[4] S. Jadach, B. F. L. Ward, and Z. Was, *Phys. Rev.* **D88** (2013), no. 11 114022, 1307.4037.

[5] G. Altarelli, R. Kleiss, and C. Verzegnassi, eds., *Z physics at LEP-1. Proceedings, Workshop, Geneva, Switzerland, September 4-5, 1989. vol. 1: Standard Physics*, 1989.

[6] F. A. Berends, R. Kleiss, and S. Jadach, *Comput. Phys. Commun.* **29** (1983) 185–200.

[7] E. Richter-Was and Z. Was, *Eur. Phys. J.* **C76** (2016), no. 8 473, 1605.05450.

[8] E. Richter-Was and Z. Was, 1609.02536.

[9] J. H. Kuhn, A. Kulesza, S. Pozzorini, and M. Schulze, *Nucl. Phys.* **B727** (2005) 368–394, hep-ph/0507178.

[10] S. Jadach, B. Ward, and Z. Was, *Comput.Phys.Commun.* **130** (2000) 260–325, hep-ph/9912214.

[11] Z. Czyczula, T. Przedzinski, and Z. Was, *Eur.Phys.J.* **C72** (2012) 1988, 1201.0117.

[12] D. Yu. Bardin, M. S. Bilenky, T. Riemann, M. Sachwitz, and H. Vogt, *Comput. Phys. Commun.* **59** (1990) 303–312.

[13] A. Andonov, A. Arbuzov, D. Bardin, S. Bondarenko, P. Christova, L. Kalinovskaya, V. Kolesnikov, and R. Sadykov, *Comput. Phys. Commun.* **181** (2010) 305–312, 0812.4207.

[14] A. Akhundov, A. Arbuzov, S. Riemann, and T. Riemann, *Phys. Part. Nucl.* **45** (2014), no. 3 529–549, 1302.1395.

[15] Dizet and new version.

[16] M. Tabanashi *et al.*, *Phys. Rev.* **D98** (2018) 030001.

[17] A. Freitas *et al.*, 1906.05379.

[18] S. G. Bondarenko and A. A. Sapronov, *Comput. Phys. Commun.* **184** (2013) 2343–2350, 1301.3687.

[19] A. Arbuzov, D. Bardin, S. Bondarenko, P. Christova, L. Kalinovskaya, U. Klein, V. Kolesnikov, L. Rumyantsev, R. Sadykov, and A. Sapronov, *JETP Lett.* **103** (2016), no. 2 131–136, 1509.03052.

[20] H. Burkhardt and B. Pietrzyk, *Phys. Lett.* **B513** (2001) 46–52.

[21] E. Richter-Was and Z. Was, *Eur. Phys. J.* **C79** (2019), no. 6 480, 1808.08616.

[22] Particle Data Group Collaboration, C. Patrignani *et al.*, *Chin. Phys.* **C40** (2016), no. 10 100001.

[23] S. Alioli *et al.*, *Eur. Phys. J.* **C77** (2017), no. 5 280, 1606.02330.

[24] W. J. Marciano and A. Sirlin, *Phys. Rev.* **D22** (1980) 2695, [Erratum: Phys. Rev.D31,213(1985)].

[25] D. R. Yennie, S. C. Frautschi, and H. Suura, *Annals Phys.* **13** (1961) 379–452.

[26] M. Chiesa, F. Piccinini, and A. Vicini, 1906.11569.

[27] D. Yu. Bardin, P. K. Khristova, and O. M. Fedorenko, *Nucl. Phys.* **B175** (1980) 435–461.

[28] D. Yu. Bardin, P. K. Khristova, and O. M. Fedorenko, *Nucl. Phys.* **B197** (1982) 1–44.

[29] A. Sirlin, *Phys. Rev.* **D22** (1980) 971–981.

[30] F. Jegerlehner, 1711.06089.

[31] A. Blondel, J. Gluza, S. Jadach, P. Janot, and T. Riemann, eds., *Theory report on the 11th FCC-ee workshop*, 2019.

[32] T. Przedzinski, E. Richter-Was, and Z. Was, *Eur. Phys. J.* **C74** (2014), no. 11 3177, 1406.1647.

[33] N. Davidson, G. Nanava, T. Przedzinski, E. Richter-Was, and Z. Was, *Comput.Phys.Commun.* **183** (2012) 821–843, 1002.0543.

[34] Z. Was and S. Jadach, *Phys. Rev.* **D41** (1990) 1425.

[35] J. C. Collins and D. E. Soper, *Phys. Rev.* **D16** (1977) 2219.

A EW schemes

There are several ingredients that goes into definition of *EW schemes*

- Choice of the input parameters
- Renormalisation scheme
- Treatment of other corrections: treatment of self-energy corrections in the propagator (running or fixed width), *on-mass-shell* or *pole* mass in the propagator.
- Something more?

Formally, at the lowest EW order, only three parameters can be set, others are calculated using Standard Model constraints, following structure of $SU(2)\times U(1)$ group. One of such constraint is given in formula (38). The most common choices at hadron colliders, following report [23], are G_μ *scheme* (G_μ, M_Z, M_W) and $\alpha(0)$ *scheme* $(\alpha(0), M_Z, M_W)$. There exists by now family of different modifications of G_μ *scheme*, see discussion in [23], and they are considered as preferred schemes for hadron collider physics.

The Monte Carlo generators usually allow user to define set of input parameters (α, M_Z, M_W), (α, M_Z, G_μ) or (α, M_Z, s_W^2). However within this flexibility, formally multiplicative factor in the Z-boson propagator $\chi_Z(s)$, see formula (20), is always kept to be equal to 1. The

$$\frac{G_\mu \cdot M_z^2 \cdot 16 \cdot c_W^2 \cdot s_W^2}{\sqrt{2}\cdot 8\pi \cdot \alpha} = 1; \tag{8}$$

where $s_W^2 = 1 - m_W^2/m_Z^2$ and $c_W^2 = 1 - s_W^2$. This term is quite often absent in the programs code. Whichever the choice of parameters set is used as primary ones, the others are adjusted to match the constraint (8), regardless if they fall outside their measurement uncertainties or not.

Let us recall, that the calculations of EW corrections available in `Dizet` library work with somewhat different convention of the $\alpha(0)$ *scheme*, defined by the set of input parameters $(\alpha(0), G_\mu, M_Z)$, then M_W is calculated iterating formula (35), which formally brings it beyond EW LO scheme. The value of s_W^2 is calculated from (39) and the EW LO relation (38) does not hold anymore.

For the comparisons performed here we consider following schemes:

A.1 EW scheme: $\alpha(0), G_\mu, M_Z$

This choice will be denoted as $\alpha(0)$ v0 scheme.

Here are formulas to recalculate remaining EW parameters:

$$d2 = \frac{\sqrt{2}\cdot 8\pi \cdot \alpha}{G_\mu \cdot M_z^2} \tag{9}$$

$$s_W^2 = (-1 + \sqrt{1 - d2/4})/2 \tag{10}$$

$$m_W^2 = (1 - s_W^2)\cdot M_Z^2 \tag{11}$$

A.2 EW scheme: $\alpha(0), M_W, M_Z$

This choice will be denoted as $\alpha(0)$ v1 scheme.

Here are formulas to recalculate remaining EW parameters:

$$\begin{aligned} s_W^2 &= 1 - M_W^2/M_Z^2 \\ g2 &= 4\cdot\pi\cdot\alpha/s_W^2 \\ G_\mu &= \sqrt{2}\cdot g2/8/M_W^2 \end{aligned} \tag{12}$$

A.3 EW scheme: G_μ, M_Z, M_W

This choice will be denoted as G_μ scheme.

A convenient set of parameters that describes EW processes at hadron colliders is (G_μ, M_W, M_Z), the so called G_μ scheme. The Fermi constant G_μ measured in muon decay naturally parametrize the CC interaction, while the W and Z masses fix the scale of EW phenomena and the mixing with hyper-charge field. A drawback of this choice is the fact that the coupling of real photons to charge particles is computed from the inputs and in lowest order is equal to

$$\alpha = G_\mu \sqrt{2} M_W^2 (1 - M_W^2/M_Z^2)/\pi \sim 1/132 \tag{13}$$

much larger that the fine structure constant $\alpha(0) = 1/137$, which is a natural value for an on-shell photons.

This drawback can be circumvented by a use of modified G_μ scheme when only LO couplings are re-expressed in terms of α

$$\alpha_{QED} = \alpha(0) \to \alpha(1 - \Delta r) \tag{14}$$

and the Sirlin's parameter Δr [24], representing the complete NLO EW radiative corrections of $O(\alpha)$ to the muon decay amplitude. Both real and virtual relative corrections are calculated at the scale $O(\alpha)$, therefore such an approach may be referred as NLO at $O(\alpha G_\mu^2)$. In this scheme leading universal corrections due to the running of α and connected to the ρ parameter are absorbed in the LO couplings.

Further modifications maybe considered. For the NC DY the gauge invariant separation of complete EW radiative corrections into pure weak and QED corrections (involving virtual and real photons) is possible. Therefore, these two contributions may be considered at different scales, pure weak at $O(G_\mu^3)$, and QED still at $O(\alpha G_\mu^2)$. More refined modifications may be considered, for instance based on defining gauge invariant subsets by using the Yennie-Frautschi-Suura approach [25].

Here are formulas to calculate remaining EW parameters:

$$\begin{aligned} s_W^2 &= 1 - M_W^2/M_Z^2 \\ g2 &= 8 \cdot G_\mu \cdot M_W^2/\sqrt{2} \\ \alpha &= g2 \cdot s_W^2/4/\pi \end{aligned} \tag{15}$$

A.4 EW scheme: $\alpha(0), s_W^2, M_Z$

This choice will be denoted as sin^2_{eff} v1 scheme.

Text to be written, based on recent publication [26]

A.5 EW scheme: G_μ, s_W^2, M_Z

This choice will be denoted as sin^2_{eff} v2 scheme.

Text to be written, based on recent publication [26]

A.6 Benchmark initialisation

Benchmark initialisation of the different EW schemes are chosen such that they share value of one or more input parameters which facilitate comparison of the cross-sections or asymmetries at the EW LO. The $\alpha(0)$ v0 and v1 share same value of α, the $\alpha(0)$ v1 and G_μ schemes same value of M_W (and therefore s_W^2). In all three cases the M_Z and Γ_Z are the same. Common is also choice for the fermion masses, quarks and leptons and for the Higgs boson mass, as shown in Table 12.

Table 12: Values of fermions and Higgs boson massed used for calculating EW corrections.

Parameter	Mass (GeV)	Description
m_e	5.1099907e-4	mass of electron
m_μ	0.1056583	mass of muon
m_τ	1.7770500	mass of tau
m_u	0.0620000	mass of up-quark
m_d	0.0830000	mass of down-quark
m_c	1.5000000	mass of charm-quark
m_s	0.2150000	mass of strange-quark
m_b	4.7000000	mass of bottom-quark
m_t	173.0	mass of top quark
m_H	125.0	mass of Higgs boson

Table 13: The EW parameters used at tree-level EW, with on-mass-shell definition (LEP convention).

Parameter	$(\alpha(0), G_\mu, M_Z)$ $\alpha(0)$ v0	$(\alpha(0), M_W, M_Z)$ $\alpha(0)$ v1	(G_μ, M_Z, M_W) G_μ	$(\alpha(0), s_W^2, M_Z)$ $\sin^2_{eff}$ v1	(G_μ, s_W^2, M_Z) sin^2_{eff} v2
M_Z (GeV)	91.1876	91.1876	91.1876	91.1876	91.1876
Γ_Z (GeV)	2.4952	2.4952	2.4952	2.4952	2.4952
Γ_W (GeV)	2.085	2.085	2.085	2.085	2.085
$1/\alpha$	137.035999139	137.035999139	132.23323	137.035999139	128.744939484
α	0.007297353	0.007297353	0.007562396	0.007297353	0.007767296
G_μ (GeV^{-2})	$1.1663787 \cdot 10^{-5}$	$1.1254734 \cdot 10^{-5}$	$1.1663787 \cdot 10^{-5}$	$1.09580954 \cdot 10^{-5}$	$1.1663787 \cdot 10^{-5}$
M_W (GeV)	80.93886	80.385	80.385	79.93886984	79.93886984
s_W^2	0.2121517	0.2228972	0.2228972	0.231499	0.231499
$\frac{G_\mu \cdot M_z^2 \cdot 16 c_W^2 s_W^2}{\sqrt{2} \cdot 8\pi \cdot \alpha} = 1.0$ $s_W^2 = 1 - m_W^2/m_Z^2$	$\to s_W^2, M_W$	$\to G_\mu, s_W^2$	$\to \alpha, s_W^2$	$\to G_\mu, m_W$	$\to \alpha, m_W$
$\alpha_s(M_Z)$	0.120178900000	0.120178900000	0.120178900000	0.120178900000	0.120178900000

Table 14: The EW parameters used at tree-level EW, with pole definition of the Z, W masses.

Parameter	$(\alpha(0), G_\mu, M_Z)$ $\alpha(0)$ v0	$(\alpha(0), M_W, M_Z)$ $\alpha(0)$ v1	(G_μ, M_Z, M_W) G_μ	$(\alpha(0), s_W^2, M_Z)$ $\sin^2_{eff}$ v1	(G_μ, s_W^2, M_Z) sin^2_{eff} v2
M_Z (GeV)	91.15348	91.15348	91.15348	91.15348	91.15348
Γ_Z (GeV)	2.494266	2.494266	2.494266	2.494266	2.494266
Γ_W (GeV)	2.085	2.085	2.085	2.085	2.085
$1/\alpha$	137.035999139	137.035999139	132.3572336357709	137.035999139	128.84133952
α	0.007297353	0.007297353	0.007555311	0.007297353	0.007761484
G_μ (GeV^{-2})	$1.1663787 \cdot 10^{-5}$	$1.126555497 \cdot 10^{-5}$	$1.1663787 \cdot 10^{-5}$	$1.09663005 \cdot 10^{-5}$	$1.1663787 \cdot 10^{-5}$
M_W (GeV)	80.91191	80.35797	80.35797	79.90895881	79.90895881
s_W^2	0.21208680	0.22283820939	0.22283820939	0.231499	0.231499
$\frac{G_\mu \cdot M_z^2 \cdot 16 c_W^2 s_W^2}{\sqrt{2} \cdot 8\pi \cdot \alpha} = 1.0$ $s_W^2 = 1 - m_W^2/m_Z^2$	$\to s_W^2, M_W$	$\to G_\mu, s_W^2$	$\to \alpha, s_W^2$	$\to G_\mu, m_W$	$\to \alpha, m_W$
$\alpha_s(M_Z)$	0.120178900000	0.120178900000	0.120178900000	0.120178900000	0.120178900000

B Improved Born Approximation

Comment: Content of this section is taken from [21].

At LEP times, to match higher order QED effects with the loop corrections of electroweak sector, concept of electroweak form factors was introduced [5]. This arrangement was very beneficial and enabled common treatment of one loop electroweak effects with not only higher order QED corrections including bremsstrahlung, but also to incorporate higher order loops into Z and photon propagators, see eg. documentation of `KKMC` Monte Carlo [4] or `Dizet` [2]. Such description has its limitations for the LHC applications, but for the processes of the Drell-Yan type with a moderate virtuality of produced lepton pairs is expected to be useful, even in case when high p_T jets are present. For the LEP applications [1], the EW form factors were used together with multiphoton bremsstrahlung amplitudes. For the purpose of this Section we discuss use for parton level Born processes only, no QED ISR/FSR.

The approximation which is discussed here is called *Improved Born Approximation* (IBA) [2]. It absorbs some or all of higher order EW corrections by redefinition of couplings and propagators in the Born spin amplitude, and allows to calculate doubly deconvoluted observables, like various cross-sections and asymmetries.

The initial/final QCD and QED corrections, form separately gauge invariant subsets of diagrams [2]. The QED subset consists of QED-vertices, $\gamma\gamma$ and γZ boxes, bremsstrahlung diagrams. Fermionic self-energies have to be also taken into account. Corresponding subset can be constructed also for the initial/final QCD corrections. All the remaining corrections contribute to the IBA: purely EW loop and boxes and *internal* QCD corrections (lineshape corrections). They can be split into two more gauge-invariant subsets, giving rise to two *improved (or dressed)* amplitudes: (i) improved γ exchange amplitude with running QED coupling where only fermion loops contribute and (ii) improved Z-boson exchange amplitude with four, in general complex, *EW form factors*: $\rho_{\ell f}$, $\mathscr{K}_\ell$, $\mathscr{K}_f$, $\mathscr{K}_{\ell f}$. Components of those corrections are as following:

- Corrections to photon propagator, where only fermion loops contribute, so called vacuum-polarisation corrections.
- Corrections to Z-boson propagator and couplings, called EW form-factors.
- Contribution from the purely weak boxes, the WW and ZZ diagrams. They are negligible at the Z-peak (suppressed by the factor $(s-M_Z^2)/s$), but very important at higher energies. They enter as corrections to form-factors and introduce dependence on $\cos\theta$ of scattering angle.
- Mixed $O(\alpha\alpha_s)$ corrections which originate from gluon insertions to the fermionic components of bosonic self-energies. They also enter as corrections to all form-factors.

Below, to define notation we present formula of the Born spin amplitude $\mathscr{A}^{Born}$. We recall here conventions from [2]. Let us start with defining the lowest order coupling constants (without EW corrections) of the Z boson to fermions: $s_W^2 = 1 - m_W^2/m_Z^2$ defines weak angle $\sin\theta_W^2$ in the on-shell scheme and $T_3^{\ell,f}$ third component of the isospin. The vector v_ℓ, v_f and axial a_ℓ, a_f couplings for leptons and quarks are defined with the formulae below[3]

$$\begin{aligned} v_\ell &= (2\cdot T_3^\ell - 4\cdot q_\ell \cdot s_W^2)/\Delta, \\ v_f &= (2\cdot T_3^f - 4\cdot q_f \cdot s_W^2)/\Delta, \\ a_\ell &= (2\cdot T_3^\ell)/\Delta, \\ a_f &= (2\cdot T_3^f)/\Delta. \end{aligned} \tag{16}$$

where

$$\Delta = \sqrt{16\cdot s_W^2\cdot(1-s_W^2)}. \tag{17}$$

With this notation, spin amplitude for the $q\bar{q} \to Z/\gamma^* \to \ell^+\ell^-$, denoted as $\mathscr{A}^{Born}$, can be written as:

$$\begin{aligned} \mathscr{A}^{Born} = \frac{\alpha}{s}\{ \quad & [\bar{u}\gamma^\mu v g_{\mu\nu}\bar{v}\gamma^\nu u]\cdot(q_\ell\cdot q_f)\cdot\chi_\gamma(s) + [\bar{u}\gamma^\mu v g_{\mu\nu}\bar{v}\gamma^\nu u\cdot(v_\ell\cdot v_f) \\ & + \bar{u}\gamma^\mu v g_{\mu\nu}\bar{v}\gamma^\nu\gamma^5 u\cdot(v_\ell\cdot a_f) + \bar{u}\gamma^\mu\gamma^5 v g_{\mu\nu}\bar{v}\gamma^\nu u\cdot(a_\ell\cdot v_f) + \bar{u}\gamma^\mu\gamma^5 v g_{\mu\nu}\bar{v}\gamma^\nu\gamma^5 u\cdot(a_\ell\cdot a_f)]\cdot\chi_Z(s) \quad \}, \end{aligned} \tag{18}$$

[3] We will use "ℓ" for lepton, and "f" for quarks.

where u, v denote fermion spinors, Z-boson and photon propagators are defined respectively as:

$$\chi_\gamma(s) = 1, \tag{19}$$

$$\chi_Z(s) = \frac{G_\mu \cdot M_z^2 \cdot \Delta^2}{\sqrt{2} \cdot 8\pi \cdot \alpha} \cdot \frac{s}{s - M_Z^2 + i \cdot \Gamma_Z \cdot s/M_Z}. \tag{20}$$

Then, we redefine vector and axial couplings introducing EW form-factor corrections $\rho_{\ell f}, \mathscr{K}_\ell(s,t), \mathscr{K}_f(s,t), \mathscr{K}_{\ell f}$ as the following:

$$\begin{aligned} v_\ell &= (2 \cdot T_3^\ell - 4 \cdot q_\ell \cdot s_W^2 \cdot \mathscr{K}_\ell(s,t))/\Delta, \\ v_f &= (2 \cdot T_3^f - 4 \cdot q_f \cdot s_W^2 \cdot \mathscr{K}_f(s,t))/\Delta, \\ a_\ell &= (2 \cdot T_3^\ell)/\Delta, \\ a_f &= (2 \cdot T_3^f)/\Delta. \end{aligned} \tag{21}$$

Normalisation correction Z_{V_Π} to Z-boson propagator is defined as

$$Z_{V_\Pi} = \rho_{\ell f}(s,t)\ . \tag{22}$$

Vacuum polarisation corrections Γ_{V_Π} to γ propagator are expressed as

$$\Gamma_{V_\Pi} = \frac{1}{2 - (1 + \Pi_{\gamma\gamma}(s))}, \tag{23}$$

where $\Pi_{\gamma\gamma}(s)$ denotes vacuum polarisation corrections to photon propagator. Both Γ_{V_Π} and Z_{V_Π} are multiplicative correction factors. The $\rho_{\ell f}(s,t)$ can be also absorbed as multiplicative factor into definition of vector and axial couplings.

The EW form-factors $\rho_{\ell f}, \mathscr{K}_\ell(s,t), \mathscr{K}_f(s,t), \mathscr{K}_{\ell f}$ are functions of two Mandelstam invariants (s,t) due to the WW and ZZ box contributions. The Mandelstam variables are defined such that they satisfy the identity

$$s + t + u = 0 \quad where \quad t = -\frac{s}{2}(1 - \cos\theta) \tag{24}$$

and $\cos\theta$ is the cosinus of the scattering angle, i.e. angle between incoming and outgoing fermion directions.

Note, that in this approach the mixed EW and QCD loop corrections, originating from gluon insertions to fermionic components of bosonic self-energies, are included in $\Gamma_{V_\Pi}, Z_{V_\Pi}$ factors.

One has to take also into account the angle dependent double-vector coupling corrections which break factorisation of the couplings shown in (18), into ones associated with either Z boson production or decay. This requires introducing mixed term:

$$\begin{aligned} vv_{\ell f} = \quad & \frac{1}{v_\ell \cdot v_f}[(2 \cdot T_3^\ell)(2 \cdot T_3^f) - 4 \cdot q_\ell \cdot s_W^2 \cdot \mathscr{K}_f(s,t)(2 \cdot T_3^\ell) - 4 \cdot q_f \cdot s_W^2 \cdot \mathscr{K}_\ell(s,t)(2 \cdot T_3^f) \\ & + (4 \cdot q_\ell \cdot s_W^2)(4 \cdot q_f \cdot s_W^2)\mathscr{K}_{\ell f}(s,t)]\frac{1}{\Delta^2}. \end{aligned} \tag{25}$$

Finally, we can write the spin amplitude for Born with EW corrections, $\mathscr{A}^{Born+EW}$, as:

$$\begin{aligned} \mathscr{A}^{Born+EW} = \quad & \frac{\alpha}{s}\{[\bar{u}\gamma^\mu v g_{\mu\nu} \bar{v}\gamma^\nu u] \cdot (q_\ell \cdot q_f)] \cdot \Gamma_{V_\Pi} \cdot \chi_\gamma(s) + [\bar{u}\gamma^\mu v g_{\mu\nu} \bar{v}\gamma^\nu u \cdot (v_\ell \cdot v_f \cdot vv_{\ell f}) \\ & + \bar{u}\gamma^\mu v g_{\mu\nu} \bar{v}\gamma^\nu\gamma^5 u \cdot (v_\ell \cdot a_f) + \bar{u}\gamma^\mu\gamma^5 v g_{\mu\nu} \bar{v}\gamma^\nu u \cdot (a_\ell \cdot v_f) + \bar{u}\gamma^\mu\gamma^5 v g_{\mu\nu} \bar{v}\gamma^\nu\gamma^5 u \cdot (a_\ell \cdot a_f)] \cdot Z_{V_\Pi} \cdot \chi_Z(s)\}. \end{aligned} \tag{26}$$

The EW form factor corrections: $\rho_{\ell f}, \mathscr{K}_\ell, \mathscr{K}_f, \mathscr{K}_{\ell f}$ can be calculated using `Dizet` library. This library is also used to calculate vacuum polarisation corrections to photon propagator $\Pi_{\gamma\gamma}$. For the case of pp collisions we do not introduce QCD corrections to vector and axial coupling in initial fermion vertex, as they will be included later as a part of the QCD NLO calculations of the initial state convolution with proton structure functions.

The *Improved Born Approximation* uses spin amplitude $\mathscr{A}^{Born+EW}$ of Eq. (26) and $2 \to 2$ body kinematics to define differential cross-section with EW corrections for $q\bar{q} \to Z/\gamma^* \to ll$ process. Presented above formulae very closely follow the approach taken for implementation[4] of EW corrections to `KKMC` Monte Carlo [4].

[4]Compatibility with this program is also part of the motivation, why we leave updates for the `Dizet` library to the forthcoming work. `Dizet 6.21` is also well documented.

For completeness let us note that above discussion was presented for scattering process, however one may be interested in the decay process only. For this, *effective couplings* of Z-decay are often introduced; there are complex-valued constants as well.

The ratio of effective vector and axial couplings defines g_Z^f (here we use “f” for quark or lepton)

$$g_Z^f = \frac{v_Z^f}{a_Z^f} = 1 - 4|q_f|(K_Z^f s_W^2 + I_f^2) \tag{27}$$

with

$$I_f^2 = \alpha^2(s)\frac{35}{18}[1 - \frac{8}{3}Re(K_Z^f)s_W^2]. \tag{28}$$

and the flavour dependent *effective weak mixing angles* as

$$\sin^2\theta_{eff}^f = Re(\mathscr{K}_Z^f)s_W^2 + I_f^2 \tag{29}$$

C The s dependent Z-boson width

Comments:
This material is a placeholder for more advanced studies, for now it is just quantifying a problem.

- *Using M_Z, Γ_Z values as measured at LEP with fixed width propagator $\chi_Z(s)$ leads to an effect on the level of $5\cdot 10^{-4}$ on A_{fb} integrated in the mass range $80-100$ GeV, with respect to nominal predictions of propagator with running width. See Fig. 10 and Table 17.*
- *The "pole mass" convention is introducing shifted masses, see Table 14, which are then used with fixed width propagator. However it is just mathematical transformation as detailed in Eq.(**??**). This to be equivalent "to on-shell" convention, should also take into account normalisation factor N_Z which usually is not done.*
- *The question is however, how in the "pole mass" convention, resummation of the fermionic loop corrections to the propagator, which are otherwise modeled by running width in the propagator are accounted for.*
- *More material available from slides by F. Piccinini*
  `https://indico.cern.ch/event/829225/contributions/3481094/attachments/1871705/3080271/piccinini.pdf`

In formula (20) for the definition of Z propagator running width is used:

$$\chi_Z'(s) = \frac{1}{s - M_Z^2 + i\cdot\Gamma_Z\cdot s/M_Z} \tag{30}$$

is often in use.

The form-factors are calculated for the nominal value of M_Z. The so-called s-dependent width is equivalent to further (still partial) resummation of loop corrections, the boson self-energy which is s dependent. This formula was used in many analyses of LEP era.

In many Monte Carlos of LHC era, the definition of Z propagator constant width is used:

$$\chi_Z(s) = \frac{1}{s - M_Z^2 + i\cdot\Gamma_Z\cdot M_Z}. \tag{31}$$

One can ask the simple question, how analytic forms of (**??**) and (31) translate to each other. Let us start from (**??**)

$$\begin{aligned}
\chi_Z'(s) &= \frac{1}{s(1+i\cdot\Gamma_Z/M_Z) - M_Z^2} \\
&= \frac{(1-i\cdot\Gamma_Z/M_Z)}{s(1+\Gamma_Z^2/M_Z^2) - M_Z^2(1-i\cdot\Gamma_Z/M_Z)} \\
&= \frac{(1-i\cdot\Gamma_Z/M_Z)}{(1+\Gamma_Z^2/M_Z^2)}\frac{1}{s - \frac{M_Z^2}{1+\Gamma_Z^2/M_Z^2} + i\cdot\frac{\Gamma_Z M_Z}{1+\Gamma_Z^2/M_Z^2}} \\
&= N_Z\frac{1}{s - {M_Z'}^2 + i\Gamma_Z' M_Z'} \\
M_Z' &= \frac{M_Z}{\sqrt{1+\Gamma_Z^2/M_Z^2}} \\
\Gamma_Z' &= \frac{\Gamma_Z}{\sqrt{1+\Gamma_Z^2/M_Z^2}} \\
N_Z &= \frac{(1-i\cdot\Gamma_Z/M_Z)}{(1+\Gamma_Z^2/M_Z^2)} = \frac{(1-i\cdot\Gamma_Z'/M_Z')}{(1+{\Gamma_Z'}^2/{M_Z'}^2)}
\end{aligned} \tag{32}$$

The s-dependent width in Z propagator translates into shift in Z propagator mass and width and introduction of the overall complex factor with respect to constant width definition. This last point is possibly least trivial as it

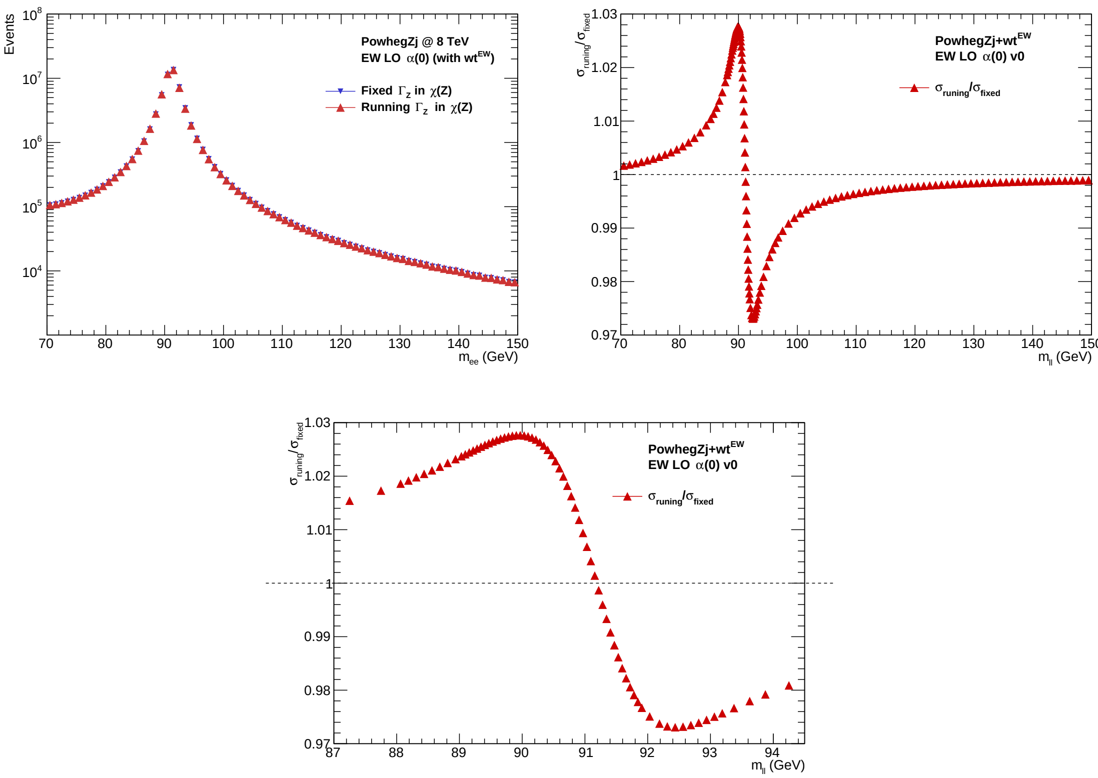

Figure 9: The line shape distribution after changing fixed to running Γ_Z in the Z-boson propagator $\chi(Z)$. I.e. using either Eq.(30) or Eq.(**??**) for the propagator, without redefining M_Z or other parameters.

effectively mean redefinition of Z coupling. That is why it can not be understood as parameter re-scaling. It points to present in higher order relations between vacuum polarization and vertex. Most of the changes are due to the term Γ_Z^2/M_Z^2 except of the overall phase which result from $1 - i \cdot \Gamma_Z/M_Z$ factor and which change the γZ interference. The shift in M_Z is by about 34 MeV downwards, and the shift in Γ_Z by 1 MeV, due the reparametrisation of the Z-boson propagator.

In Figure 9 shown is effect of changing from fixed Γ_Z to running Γ_Z scheme without shift in the M_Z value. The relative S-shape corrections are due to shift in the peak position of the line-shape and are on the level of $\pm 1\%$. In Figure 10 shown is effect on forward-backward asymmetry A_{FB}. In Table **??** shown are total, forward and backward cross-sections in a mass window, normalised to total generated sample, and forward-backward asymmetry. Results are shown for wt^{EW} applied to generated sample to reweight to different EW LO schemes, using Z-boson propagator $\chi(Z)$ with fixed or running width. The last column shows difference $\Delta A_{FB} = A_{FB}(fixed\Gamma_Z) - A_{FB}(running\Gamma_Z)$. Table 17 shows results for predictions including EW NLO+HO form-factors corrections calculated with `Dizet` library.

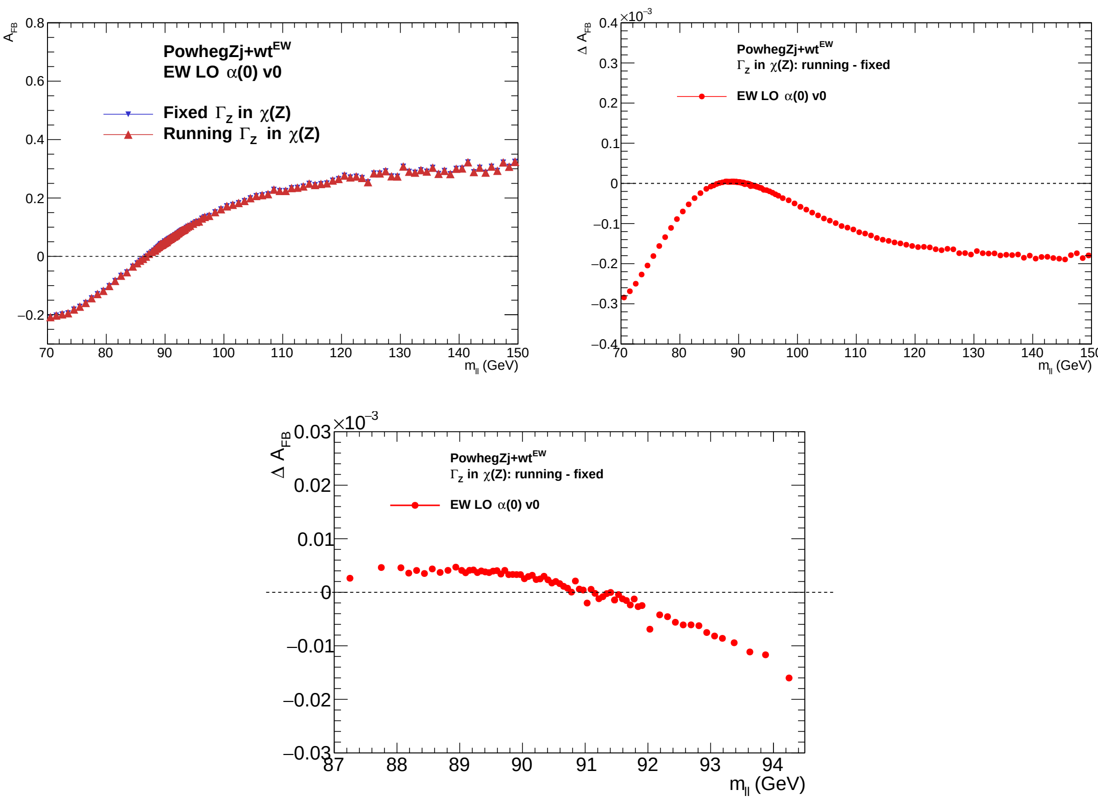

Figure 10: The difference in forward-backward asymmetry after changing fixed to running Γ_Z in the Z-boson propagator $\chi(Z)$. I.e. using either Eq.(30) or Eq.(**??**) for the propagator, without redefining M_Z or other parameters.

Table 15: The cross-sections and A_{FB} evaluated with fixed or running Z width in propagator $\chi(Z)$. Cross-section in mass window is given in fractions of total generated cross-section with `PowhegZj`. Predictions for EW LO $\alpha(0)$ `v0` scheme with s_W^2 =0.2121517.

Γ_Z in $\chi(Z)$	m_{ll} (GeV)	σ	σ_F	σ_B	$\Delta\sigma_{FB}$	A_{FB}	ΔA_{FB}
fixed	90.9876 - 91.3876	0.25193	0.13396	0.11797	0.01599	0.06346	
running		0.25356	0.13482	0.11874	0.01608	0.06343	0.00003
fixed	90.8876 - 91.4876	0.25193	0.13396	0.11797	0.01599	0.06346	
running		0.25356	0.13482	0.11874	0.01608	0.06343	0.00003
fixed	90.6876 - 91.6876	0.36371	0.19390	0.16981	0.02409	0.06623	
running		0.36317	0.19360	0.16957	0.02403	0.06616	0.00008
fixed	80 - 100	0.99486	0.52925	0.46561	0.06365	0.06398	
running		0.99507	0.52915	0.46592	0.06323	0.06354	0.00044

Table 16: The cross-sections and A_{FB} evaluated with fixed or running Z width in propagator $\chi(Z)$. Cross-section in mass window is given in fractions of total generated events. Predictions for EW LO $\alpha(0)$ `v1` scheme with s_W^2 =0.222838.

Γ_Z in $\chi(Z)$	m_{ll} (GeV)	σ	σ_F	σ_B	$\Delta\sigma_{FB}$	A_{FB}	ΔA_{FB}
fixed	90.9876 - 91.3876	0.22822	0.11906	0.10916	0.00991	0.04341	
running		0.22970	0.11983	0.10987	0.00996	0.04336	0.00005
fixed	90.8876 - 91.4876	0.22822	0.11906	0.10916	0.00991	0.04341	
running		0.22970	0.11983	0.10987	0.00996	0.04336	0.00005
fixed	90.6876 - 91.6876	0.32942	0.17235	0.15707	0.01528	0.04640	
running		0.32893	0.17208	0.15685	0.01523	0.04631	0.00009
fixed	80 - 100	0.90181	0.47077	0.43104	0.03974	0.04406	
running		0.90202	0.47067	0.43135	0.03932	0.04359	0.00047

Table 17: The cross-sections and A_{FB} evaluated with fixed or running Z width in propagator $\chi(Z)$. Cross-section in mass window is given in fractions of total generated events. Predictions for $\alpha(0)$ `v0` scheme corrected with EW NLO+HO form-factors calculated with `Dizet` library.

Γ_Z in $\chi(Z)$	m_{ll} (GeV)	σ	σ_F	σ_B	$\Delta\sigma_{FB}$	A_{FB}	ΔA_{FB}
fixed	90.9876 - 91.3876	0.24313	0.12492	0.11821	0.00672	0.02764	
running		0.24470	0.12574	0.11897	0.00677	0.02768	0.00004
fixed	90.8876 - 91.4876	0.24313	0.12492	0.11821	0.00672	0.02764	
running		0.24470	0.12574	0.11897	0.00677	0.02768	0.00004
fixed	90.6876 - 91.6876	0.35087	0.18082	0.17005	0.01077	0.03070	
running		0.35035	0.18056	0.16979	0.01077	0.03073	0.00003
fixed	80 - 100	0.96108	0.49418	0.46690	0.02727	0.02838	
running		0.96133	0.49413	0.46720	0.02694	0.02802	0.00036

D Genuine weak and line-shape corrections from `Dizet 6.XX` library

Proposed content:

- *Short introduction to* `Dizet` *package. Description of Improved Born Approximation and introduction of form-factors here if not done in main Sections.*
- *Evolution since version* `6.21`.
- *Theoretical predictions with emphasize on latest updates. Detailed tables + illustrative plots of form-factors.*
- *Theoretical and parametric uncertainties.*

D.1 Input parameters and initialisation flags

The `Dizet` package relies on the so called *on-mass-shell* (OMS) normalisation scheme [27, 28] but modifications are present. The OMS uses the masses of all fundamental particles, both fermions and bosons, electromagnetic coupling constant $\alpha(0)$ and strong coupling $\alpha_s(M_Z)$. The dependence on the ill-defined masses of the light quarks *u, d,c, s* and *b* is solved by dispersion relation, for details see [2]. Another exception is W-boson mass M_W, which still can be predicted with better theoretical error than experimentally measured values, exploiting the very precise knowledge of the Fermi constant in μ-decay G_μ. For this reasons, M_W is usually replaced by G_μ.

The knowledge about the hadronic vacuum polarisation is contained in the quantity denoted as $\Delta\alpha_h^{(5)}(M_Z)$, which is treated as one of the input parameters. It can be either computed from quark masses or, preferably, fitted to experimental low energy $e^+e^- \to hadrons$ data.

The two important constants used are therefore: $\alpha(0)$ - electromagnetic coupling α in Thomson limit and G_μ- Fermi constant in μ-decay. The following parameters are also passed to main `Dizet` subroutine:

$$M_W,\ M_Z,\ m_t,\ \Delta\alpha_h^{(5)}(M_Z),\ \alpha_s(M_Z). \tag{33}$$

Note that the above list is over-complete, only two out of three parameters

$$G_\mu,\ M_W,\ M_Z \tag{34}$$

are independent. They can be selected with appropriate flags setting. The only meaningful choice implemented in `Dizet` library, for calculating EW corrections at the Z-resonance, is to use G_μ and M_Z as input parameters, then calculate M_W.

The M_W is calculated iteratively from the following equation

$$M_W = \frac{M_Z}{\sqrt{2}}\sqrt{1+\sqrt{1-\frac{4A_0^2}{M_Z^2(1-\Delta r)}}}, \tag{35}$$

where

$$A_0 = \sqrt{\frac{\pi\alpha(0)}{\sqrt{2}G_\mu}}. \tag{36}$$

The Sirlin's parameter Δr [29]

$$\Delta r = \Delta\alpha(M_Z) + \Delta r_{EW} \tag{37}$$

is also calculated iteratively, and the definition of Δr_{EW} involves re-summation and higher order corrections. Since this term implicitly depends on M_W and M_Z iterative procedure is needed. The resummation term in formula (37) is not formally justified by renormalisation group arguments, correct generalization is to compute higher order corrections, see more discussion in [2].

Note that once the M_W is recalculated with formula (35), the Standard Model relationship between the weak and electromagnetic couplings

$$G_\mu = \frac{\pi\alpha}{\sqrt{2}M_W^2\sin^2\theta_W} \tag{38}$$

Table 18: The `Dizet` initialisation flags: defaults in different versions.

Input NPAR()	Internal flag	Dizet 6.21 Defaults in [12]	Dizet v6.42 Defaults in [3]	Dizet v6.45	Comments
NPAR(1)	IHVP	1	1	5	$\Delta\alpha_{had}^{(5)}$ param. from [30] in v6.45
NPAR(2)	IAMT4	4	4	8	New devellopment in v6.45
NPAR(3)	IQCD	3	3	3	
NPAR(4)	IMOMS	1	1	1	
NPAR(5)	IMASS	0	0	0	
NPAR(6)	ISCRE	0	0	0	
NPAR(7)	IALEM	3	3	3	
NPAR(8)	IMASK	0	0	0	Not used since v6.21
NPAR(9)	ISCAL	0	0	0	
NPAR(10)	IBARB	2	2	2	
NPAR(11)	IFTJR	1	1	1	
NPAR(12)	IFACR	0	0	0	
NPAR(13)	IFACT	0	0	0	
NPAR(14)	IHIGS	0	0	0	
NPAR(15)	IAMFT	1	3	3	
NPAR(16)	IEWLC	1	1	1	
NPAR(17)	ICZAK	1	1	1	
NPAR(18)	IHIG2	1	1	1	
NPAR(19)	IALE2	3	3	3	
NPAR(20)	IGREF	2	2	2	
NPAR(21)	IDDZZ	1	1	1	
NPAR(22)	IAMW2	0	0	0	
NPAR(23)	ISFSR	1	1	1	
NPAR(24)	IDMWW	0	0	0	
NPAR(25)	IDSWW	0	0	0	

is not fulfilled anymore, unless the G_μ is redefined and not taken at the measured value. This is an approach of some EW LO schemes, but not the one used by `Dizet` and it requires keeping complete expression for $\chi_Z(s)$ propagator in formula for spin amplitude (26), as defined by formula (20).

In the OMS renormalisation scheme the weak mixing angle is defined uniquely through the gauge-boson masses:

$$\sin^2\theta_W = s_W^2 = 1 - \frac{M_W^2}{M_Z^2}. \tag{39}$$

With this scheme, measuring $\sin^2\theta_W$ will be equivalent to indirect measurement of M_W^2 through the relation (39).

Let us return to `Dizet` scheme. After M_W is computed, the list of input parameters of main subroutine is fully specified.

In Table 12 and 13 collected are numerical values for all parameters used in the number presented below (folow collumn with EW scheme $\alpha(0)$ v0 in Table 13).

Default configurations of the initialisation flags, corresponding to each major version of `Dizet` library, are collected in Table 18. Evolution of flags `IAMT4` and `IAMFT` corresponds to improved calculations for fermionic loop corections became gradually available. Evolution of `IHVP` corresponds to including much improved parametrisation of the $\Delta\alpha_{had}^{(5)}$ corrections.

Table 19: The `Dizet` v6.45 recalculated parameters: masses, couplings, etc.., with initialisation as in Tables 18, 12 and 13.

Parameter	Value	Description
$\alpha_{QED}(M_Z^2)$	0.0077549256	calculated using $\Delta\alpha_h^{(5)}(m_Z^2)$ from [30]
$1/\alpha_{QED}(M_Z^2)$	128.950302056	
M_W (GeV)	80.3589356	W mass
$ZPAR(1) = \delta r$	0.03640338	the loop corrections to G_μ
$ZPAR(2) = \delta r_{rem}$	0.01167960	the remainder contribution $O(\alpha)$
$ZPAR(3) = s_W^2$	0.22340108	weak mixing angle defined by weak masses
$ZPAR(4) = G_\mu$ (GeV^{-2})	$1.16614173 \cdot 10^{-5}$	G_μ with loop correct.
$ZPAR(6) = \sin^2\theta^{\ell}_{eff}(M_Z^2)$	0.231499	effective weak mixing angle
$ZPAR(9) = \sin^2\theta^{up}_{eff}(M_Z^2)$	0.231392	effective weak mixing angle
$ZPAR(10) = \sin^2\theta^{down}_{eff}(M_Z^2)$	0.231265	effective weak mixing angle
$ZPAR(14) = \sin^2\theta^{bottom}_{eff}(M_Z^2)$	0.232733	effective weak mixing angle

D.2 Predictions: masses, couplings, EW form-factors

Table 19 collects few benchmark numbers for masses and couplings as calculated by `Dizet 6.45`, with initialisation as in Tables 18, 12 and 13.

Figure 11 shows real parts of the EW form-factors: $\rho_{\ell f}(s,t)$, $\mathscr{K}_f(s,t)$, $\mathscr{K}_\ell(s,t)$, $\mathscr{K}_{\ell f}(s,t)$, for a few values of $\cos\theta$, representing scattering angle between incoming quark and outgoing lepton directions in the centre-of-mass frame of outgoing lepton pairs. The Mandelstam variables (s,t) relate to invariant mass and scattering angle of outgoing leptons as defined in Eq. (24). The $\cos\theta$ dependence of the form-factors is due to box corrections and is more sizeable for the up-quarks.

Note, that at the peak of Z-boson, Born like couplings are not sizeably modified, form-factors are close to 1 and no numerically significant angular dependence is visible. At lower virtualities corrections seem to be larger because Z-boson contributions is non resonant and virtual corrections are by comparison larger. In this region of the phase-space Z-boson is anyway dominated by the contribution from virtual photon. Above the peak, contribution of WW boxes and later also ZZ boxes become gradually sizable and the dependence on $\cos\theta$ angle also appears. Those contributions become double resonant.

D.3 Theoretical and parametric uncertainties

D.3.1 Running $\alpha(s)$

Fermionic loop insertion to the photon propagator, i.e. vacuum polarisation corrections, are summed together as multiplicative factor of formula (23) to the photonic Born term in formula (26). It can be also interpreted as *running QED coupling* $\alpha(s)$ and expressed as

$$\alpha(s) = \frac{\alpha(0)}{1 - \Delta\alpha_h^{(5)}(s) - \Delta\alpha_\ell(s) - \Delta\alpha_t(s) - \Delta\alpha^{\alpha\alpha_s}(s)}. \tag{40}$$

Following [12], the hadronic contribution at M_Z is a significant correction: $\Delta\alpha_h^{(5)}(M_Z^2)$ = 0.0280398 and is calculated in 5-th flavour scheme making use of dispersion relation and experimental input from low energy experiments. This value has been significantly changed over years with new low-energy experiments. Recent estimates [30], which comes also with parametrised formula in very large range of s gives $\Delta\alpha_h^{(5)}(M_Z^2)$ = 0.0275762. The leptonic loop contribution $\Delta\alpha_\ell(s)$ is calculated analytically with up to the 3-loops, and is a comparably significant correction, $\Delta\alpha_\ell(M_Z)$ = 0.0314976. The other contributions are very small. The top contribution depends on the mass of the top quark, and for $m_t = 173.8$ GeV is $\Delta\alpha_t(s) = -0.585844 \cdot 10^{-4}$. The mixed two-loop $O(\alpha\alpha_s)$ corrections arising from $t\bar{t}$ loops with gluon, for the same top-quark mass and $\alpha_s = 0.119$ is $\Delta\alpha^{\alpha\alpha_s}(M_Z) = -0.103962 \cdot 10^{-4}$.

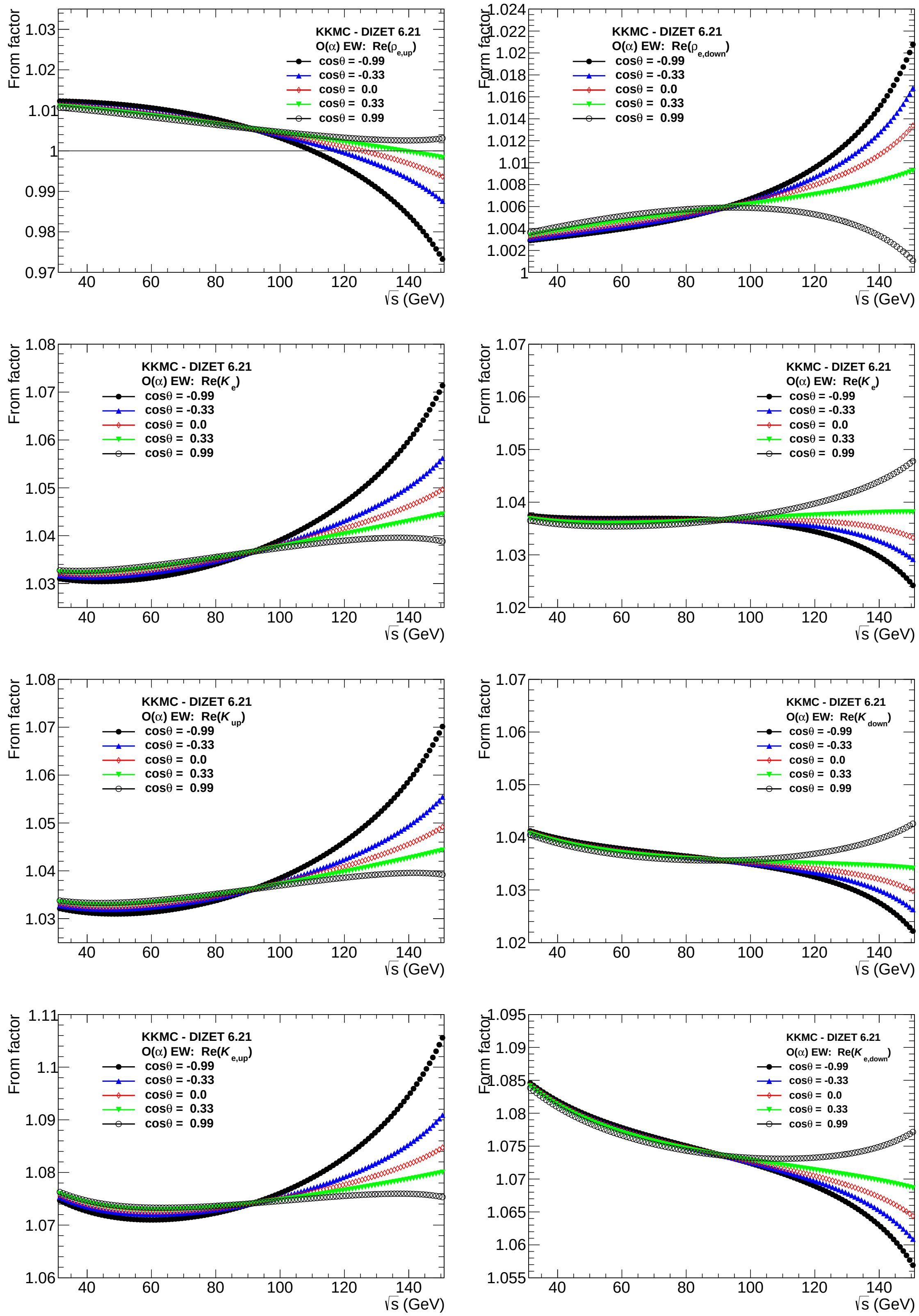

Figure 11: Real part of EW form factors for $q\bar{q} \to Z \to ee$ process: $\rho_{e,up}$, $\mathscr{K}_e$, $\mathscr{K}_{up}$ and $\mathscr{K}_{e,up}$ as a function of $\sqrt{s}$ for few values of $\cos\theta$. For u-type quark flavour left side plots are prepared and for the down-type right side plots. Note that $\mathscr{K}_e$ depend on the flavour of incoming quarks.

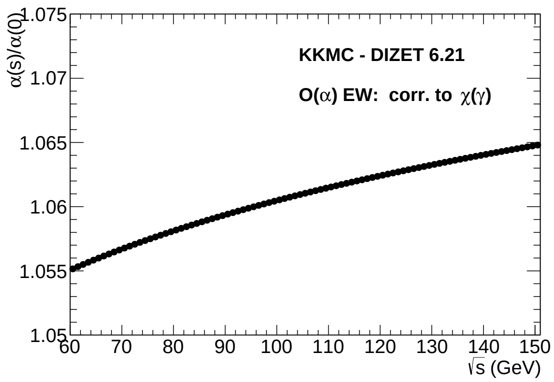

Figure 12: The vacuum polarisation correction to γ propagator, $\alpha(s)/\alpha(0)$ of formula (40), as a function of $\sqrt{s}$. *Plot should be updated with Jegerlehner 2017 parametrisation [30].*

Table 20 summarizes impact from changing predictions on the central value of $\Delta\alpha_h^{(5)}(M_Z^2)$, on the EW corrections to different quantities calculated with $\widehat{\text{D}}$izet library. Figure 12 shows $\alpha(s)/\alpha(0)$ as a function of $\sqrt{s}$.

Uncertainties on the hadronic contributions to the effective fine structure constant $\alpha(s)$ are a problem for electroweak precision physics. Because of the large 6% relative corrections between $\alpha(0)$ and $\alpha(M_Z)$, where 50% of the shift is due to non-perturbative hadronic effects, one is loosing about a factor of five orders of magnitude in precision. Present estimates of the uncertainties of SM input parameters are (from F. Jegerlehner contribution in [31]):

$$\begin{aligned}
\frac{\delta\alpha(0)}{\alpha(0)} &\sim 3.6\cdot 10^{-9}; \frac{\delta G_\mu}{G_\mu} \sim 8.6\cdot 10^{-6}; \frac{\delta M_Z}{M_Z} \sim 2.4\cdot 10^{-5}; \\
\frac{\delta\alpha(0)}{\alpha(0)} &\sim 0.9 - 1.6\cdot 10^{-4} (lost \;\; 10^5 \;\; in \;\; precision); \qquad (41) \\
\frac{\delta M_W}{M_W} &\sim 1.5\cdot 10^{-4}; \frac{\delta m_t}{m_t} \sim 2.3\cdot 10^{-3}; \frac{\delta M_H}{M_H} \sim 1.3\cdot 10^{-3};
\end{aligned}$$
(42)

The $\alpha(M_Z)$ is the least precise among the basic input parameters: $\alpha(M_Z)$, G_μ, M_Z. The present uncertainties on hadronic corrections $\delta\alpha(M_Z)$ = 0.00020 results in the error on predictions $\delta \sin^2\theta_{eff} = 0.00007$ and $\delta M_W/M_W \sim 4.3\cdot 10^{-5}$. For comparison, the uncertainties on m_t contributes $\delta \sin^2\theta_{eff}/ = 0.000002$ and $\delta M_W/M_W \sim 3.0\cdot 10^{-5}$.

The effect of uncertainties on $\Delta\alpha_h^{(5)}(M_Z^2)$, taken as ± 0.0001 on the corrections and quantities calculated by `Dizet` are summarized in Table 21.

D.3.2 Fermionic two-loop corrections

D.3.3 Top quark mass

Table 20: The `Dizet v6.45` predictions for two different parametrisations of $\Delta\alpha_h^{(5)}(M_Z^2)$. Other flags as in Tables 18.

Parameter	$\Delta\alpha_h^{(5)}(M_Z^2) = 0.0280398$ (param. Jegerlehner 1995)	$\Delta\alpha_h^{(5)}(M_Z^2) = 0.0275762$ (param. Jegerlehner 2017)	Δ
$\alpha(M_Z^2)$	0.0077587482	0.0077549256	
$1/\alpha(M_Z^2)$	128.8867699646	128.95030224	
s_W^2	0.22356339	0.22340108	- 0.00016
$sin^2\theta_{eff}(M_Z^2)$ (lepton)	0.23166087	0.23149900	- 0.00023
$sin^2\theta_{eff}(M_Z^2)$ (up-quark)	0.23155425	0.23139248	- 0.00016
$sin^2\theta_{eff}(M_Z^2)$ (down-quark)	0.23142705	0.23126543	- 0.00016
M_W (GeV)	80.3505378	80.358936	+8.4 MeV
Δr	0.03690873	0.03640338	
Δr_{rem}	0.01168001	0.01167960	

Table 21: The `Dizet v6.45` predictions: uncertainty from $\Delta\alpha_h^{(5)}(M_Z^2 = 0.0275762)$ (param. Jegerlehner 2017)[30], varied by $\pm$ 0.0001.

Parameter	$\Delta\alpha_h^{(5)}(M_Z^2)$ - 0.0001	$\Delta\alpha_h^{(5)}(M_Z^2) = 0.0275762$	$\Delta\alpha_h^{(5)}(M_Z^2)$ + 0.0001	$\Delta/2$
$\alpha(M_Z^2)$	0.0077541016	0.0077549256	0.0077557498	
$1/\alpha(M_Z^2)$	128.9640056546	128.95030224	128.9365984574	
s_W^2	0.22336607	0.22340108	0.22343610	0.000035
$sin^2\theta_{eff}(M_Z^2)$ (lepton)	0.23146409	0.23149900	0.23153392	0.000035
$sin^2\theta_{eff}(M_Z^2)$ (up-quark)	0.23135758	0.23139248	0.23142737	0.000035
$sin^2\theta_{eff}(M_Z^2)$ (down-quark)	0.23123057	0.23126543	0.23130029	0.000035
M_W (GeV)	80.3607471	80.358936	80.357124	1.8 MeV
Δr	0.03629414	0.03640338	0.03651261	
Δr_{rem}	0.01167983	0.01167960	0.01167938	

Table 22: The `Dizet v6.45` predictions with improved treatment of two-loop corrections. Other flags as in Tables 18.

Parameter	AMT4= 4	AMT4 = 8	Δ
$\alpha(M_Z^2)$	0.0077549256	0.0077549256	
$1/\alpha(M_Z^2)$	128.9503020560	128.95030224	
s_W^2	0.22333971	0.22340108	+ 0.00006
$sin^2\theta_{eff}(M_Z^2)$ (lepton)	0.23157938	0.23149900	-0.00008
$sin^2\theta_{eff}(M_Z^2)$ (up-quark)	0.23147290	0.23139248	-0.00008
$sin^2\theta_{eff}(M_Z^2)$ (down-quark)	0.23134590	0.23126543	-0.00008
M_W (GeV)	80.361846	80.358936	- 2.9 MeV
Δr	0.03640338	0.03640338	
Δr_{rem}	0.01167960	0.01167960	

Table 23: The `Dizet v6.45` predictions: uncertainty from changing top-quark mass by $\pm$0.5 GeV. Other flags as in Tables 18.

Parameter	m_t - 0.5 GeV	m_t = 173.0 GeV	m_t + 0.5 GeV	$\Delta/2$
$\alpha(M_Z^2)$	0.0077549221	0.0077549256	0.0077549291	
$1/\alpha(M_Z^2)$	128.9503600286	128.95030224	128.9502446106	
s_W^2	0.22345908	0.22340108	0.22334300	0.000058
$sin^2\theta_{eff}(M_Z^2)$ (lepton)	0.23151389	0.23149900	0.23148410	0.000016
$sin^2\theta_{eff}(M_Z^2)$ (up-quark)	0.23140736	0.23139248	0.23137758	0.000016
$sin^2\theta_{eff}(M_Z^2)$ (down-quark)	0.23128031	0.23126543	0.23125053	0.000016
M_W (GeV)	80.355935	80.358936	80.361941	3 MeV
Δr	0.03658500	0.03640338	0.03622132	
Δr_{rem}	0.01167011	0.01167960	0.01168907	

E TauSpinner with EW weights

Comment: Content of this Section was published in [21].

The TauSpinner package was initially created as a tool to correct with per-event weight longitudinal spin effects in the generated event samples including τ decays. Implemented there algorithms turned out to be of more general usage. They provide effective approach using reweighting technique to modify matrix elements of the hard processes used in Monte Carlo programs for event production and decay. The most recent summary on its algorithms and their applications is given in [**?**]. The possibility to introduce one-loop electroweak corrections from SANC library [13] in case of Drell-Yan production of the Z-boson became available in TauSpinner since [32]. This implementation allowed to introduce per-event weight calculated using pre-tabulated EW corrections for each individual spin configurations of outgoing leptons.

The implementation of EW corrections which is discussed in [21] and summarised here is enhanced. The TauSpinner package and algorithms are adapted to allow EW corrections from Dizet library directly into spin amplitudes and weight calculations for the Drell-Yan Z-boson production process. In [7, 8] we have shown that separating EW and QCD higher order corrections is possible and the Born-level spin amplitudes, if calculated in the adapted Mustraal frame [6], provide very good approximation of the EW LO sector even in case of NLO QCD description of the Drell-Yan processes. The EW corrections are introduced as form-factor corrections to Standard Model couplings and propagators entering Born-level spin amplitudes. This approach was very successful in analyses of LEP precision physics and we use the same strategy for the LHC precision physics around the Z-boson pole.

E.1 Born kinematic approximation and pp scattering

The solution for how to define Born-like kinematics in case of pp scattering is available in the algorithms of TauSpinner package [**?**]. The strategy assumes that hard-process history generated event is not known, in particular flavour and kinematics of incoming partons is therefore reconstructed, entirely from the kinematics of outgoing final states, reaction center of mass energy and with probabilities obtained from parton level cross-sections and PDFs. We briefly recall principles here and explain further optimisations.

E.2 Average over incoming partons flavour

Parton level Born cross-section $\sigma^{q\bar{q}}_{Born}(\hat{s},\cos\theta)$ is convoluted with the structure functions, and averaged over all possible flavours of incoming partons and all possible helicity states of outgoing leptons. The lowest order formula is given below

$$
\begin{aligned}
d\sigma_{Born}(x_1,x_2,\hat{s},\cos\theta) = \quad & \sum_{q_f,\bar{q}_f} [f^{q_f}(x_1,...)f^{\bar{q}_f}(x_2,...)d\sigma^{q_f\bar{q}_f}_{Born}(\hat{s},\cos\theta) \\
& + f^{q_f}(x_2,...)f^{\bar{q}_f}(x_1,...)d\sigma^{\bar{q}_f q_f}_{Born}(\hat{s},-\cos\theta)],
\end{aligned} \tag{43}
$$

where x_1, x_2 denote fractions of incoming parton momenta calculated from kinematics of outgoing leptons, $\hat{s} = x_1\, x_2\, s$ and f denotes parton density functions. We assume that kinematics is reconstructed from four-momenta of the outgoing leptons. The sign in front of $\cos\theta$, the cosine of the scattering angle, follows choice of the z-axis orientation being the one of the parton carrying x_1. The two possibilities are taken into account by the two terms of (43). The formula is used for calculating differential cross-section $d\sigma_{Born}(x_1,x_2,\hat{s},\cos\theta)$ of each analysed event, regardless its initial state kinematics and flavours of incoming partons which may be available in the event history entries. The formula can be used to a good approximation in case of NLO QCD spin amplitudes. The kinematics of outgoing leptons is used to construct *effective* kinematics of the Drell-Yan production process and decay, without need for information on the history of the hard-process itself. It can be constructed for events where initial state of Feynman diagrams were quark-gluon or gluon-gluon partons (as stored in the history event entries).

E.3 Effective beams kinematics

The x_1, x_2 are calculated from kinematics of outgoing leptons, following formulae of [33]

$$x_{1,2} = \frac{1}{2}\left(\pm \frac{p_z^{ll}}{4E} + \sqrt{(\frac{p_z^{ll}}{4E})^2 + 4\,(\frac{m_{ll}^2}{4E^2})^2}\ \right), \tag{44}$$

where E denotes energy of the proton beam and $p_z^{\ell\ell}$ denotes z-axis momenta of outgoing lepton pairs in the laboratory frame.

E.4 Definition of the polar angle

The $\cos\theta$, in case of $q\bar{q} \to Z \to \ell\ell$ process, can be defined as a weighted average of the angles of the outgoing leptons with respect to the beams directions [34]. It will be denoted as $\cos\theta^*$. Extending this definition to pp collisions, requires choice which direction along z-axis is of the quark and of the anti-quark, and then boosting their four-momenta into rest frame of the lepton pair system. The $\cos\theta^*$ distribution is calculated as follows:

$$\cos\theta_1 = \frac{\tau_x^{(1)} b_x^{(1)} + \tau_y^{(1)} b_y^{(1)} + \tau_z^{(1)} b_z^{(1)}}{|\vec{\tau}^{(1)}||\vec{b}^{(1)}|}, \quad \cos\theta_2 = \frac{\tau_x^{(2)} b_x^{(2)} + \tau_y^{(2)} b_y^{(2)} + \tau_z^{(2)} b_z^{(2)}}{|\vec{\tau}^{(2)}||\vec{b}^{(2)}|}, \tag{45}$$

finally

$$\cos\theta^* = \frac{\cos\theta_1 \sin\theta_2 + \cos\theta_2 \sin\theta_1}{\sin\theta_1 + \sin\theta_2} \tag{46}$$

where $\vec{\tau}^{(1)}, \vec{\tau}^{(2)}$ denote 3-vectors of outgoing leptons and $\vec{b}^{(1)}, \vec{b}^{(2)}$ denote 3-vectors of incoming beams with sign of the z-axis accordingly which term of (43) is considered. All 3-vectors are of lepton pair centre-of-mass system.

The definition of cosine polar angle (46) is a default of `TauSpinner` algorithms. Alternatively, one can use also polar angle from `Mustraal` [6] or `Collins-Soper` [35] frames. We will come later to the choice with the discussion on the preferred frame used in case of NLO QCD corrections included in the production process of generated events.

E.5 Concept of the EW weight

The EW corrections enter expression for the $\sigma_{Born}(\hat{s}, \cos\theta)$ through the definition of the vector and axial couplings and propagators of photon and Z-boson. They modify normalisation of the cross-sections, the line-shape of the Z-boson, polarisation of the outgoing leptons and asymmetries.

Given that to a good approximation we were able to factorise QCD and EW components of the cross-section we can now define per-event weight which specifically corrects for EW effects. Applying such weight allows to modify events generated with EW LO to the one including the EW corrections. This is very much the same idea as already implemented in `TauSpinner` for introducing corrections for different effects: spin correlations, production process, etc.

The per-event weight wt^{EW} is defined as ratio of the Born-level cross-sections with and without EW corrections

$$wt^{EW} = \frac{d\sigma_{Born+EW}(s, \cos\theta)}{d\sigma_{Born}(s, \cos\theta)}, \tag{47}$$

where $\cos\theta$ can be taken according to $\cos\theta^*$, $\cos\theta^{Mustraal}$ or $\cos\theta^{CS}$ definition. Introducing weight wt^{EW} allows for flexible and straightforward implementation of the higher order EW corrections using `TauSpinner` framework and form-factors calculated eg. with `Dizet` library.

The formula for wt^{EW} can be used to reweight from one to another EW LO scheme. In that case both the numerator and denominator of Eq. (47) will use lowest order $d\sigma_{Born}$, but calculated in different EW schemes.

E.6 EW corrections to doubly-deconvoluted observables

Having defined all components needed for calculating wt^{EW}, we will show now selected examples of numerical results for doubly-deconvoluted observables around the Z-pole.

The `Powheg+MiNLO` Monte Carlo, with NLO QCD and LO EW matrix elements, was used to generate $Z+j$ events with $Z \to e^+e^-$ decays in pp collisions at 8 TeV. No selection is applied to generated events, except requiring invariant mass of outgoing electrons in the range $70 < m_{ee} < 150$ GeV. For events generation, the EW parameters as shown in left-most column of Table 4, were used. The values for α and s_W^2 are close to the ones of MSbar discussed in [22]. Note that they are not at the values of precise measurements by LEP experiments at the Z-pole [1]. The initialisation with G_μ *scheme* of Table 4 is often used as a default for phenomenological studies at LHC and we will show later the estimated size of EW corrections for this setup.

To quantify the effect of the EW corrections, we reweight generated MC events to EW LO in the scheme used by the `Dizet` library and then introduce gradually EW corrections and form-factors calculated with that library. For each step appropriate numerator of the wt^{EW} is calculated, while for the denominator the EW LO $\mathscr{A}^{Born}$ matrix element is used, parameterised as in the left-most column of Table 4. The sequential steps, in which we illustrate effects of EW corrections are given below:

1. Reweight with wt^{EW}, from EW LO scheme with s_W^2= 0.23113 to EW LO scheme with s_W^2= 0.21215, see Table 4. The $\mathscr{A}^{Born}$ matrix element, Eq. (18), is used for calculating numerator of wt^{EW}.

2. As in step (1), but include EW corrections to m_W, effectively changing value of s_W^2 to s_W^2= 0.22352 in calculation of wt^{EW}. Relation of formula (38) is not obeyed anymore.

3. As in step (2), but include EW loop corrections to the normalisation of Z-boson and γ propagators, i.e. QCD/EW corrections to $\alpha(0)$ and $\rho_{\ell f}(s)$ form-factor calculated without box corrections. The $\mathscr{A}^{Born+EW}$ is used for calculating numerator of wt^{EW}.

4. As in step (3), but include EW corrections to Z-boson vector couplings: $\mathscr{K}_f, \mathscr{K}_e, \mathscr{K}_{\ell f}$, calculated without box corrections. The $\mathscr{A}^{Born+EW}$ is used for calculating numerator of wt^{EW}.

5. Replace $\rho_{\ell f}, \mathscr{K}_f, \mathscr{K}_e, \mathscr{K}_{\ell f}$ form-factors by the ones including box corrections. The $\mathscr{A}^{Born+EW}$ is used for calculating numerator of wt^{EW}.

After step (1) the predictions are according to EW LO and QCD NLO, but with different EW scheme than used originally for events generation. Then steps (2)-(5) introduce EW corrections. Step (3) effectively changes back α to be close to initial $\alpha(M_Z)$, while steps (4)-(5) effectively shift back value of s_W^2 to be close to the one used for events generation. Given the fact that EW LO scheme used for generating events has parameters already close to measured at the Z-pole, we expect the total EW corrections to the generated sample to be roughly at percent level.

In the following, we will also estimate how precise it would be to use effective Born approximation with *LEP* or *LEP with improved norm.* parametrisations instead of complete EW corrections. To obtain those predictions similar to step (1) listed above reweight is needed, but in the numerator of wt^{EW} the $\mathscr{A}^{Born}$ parametrisations as specified in the right two columns of Table 4 are used. For *LEP with improved norm.* the $\rho_{\ell,f} = 1.005$ has to be included.

The important flexibility of proposed approach is that wt^{EW} can be calculated using $d\sigma_{Born}$ in different frames: $\cos\theta^*$, `Mustraal` or `Collins-Soper`. For some observables, frame choice used for wt^{EW} calculation is not relevant at all and the simplest $\cos\theta^*$ frame can be used. We show later an example, where only using `Mustraal` frame for the wt^{EW} calculation leads to correct results of the reweighting procedure.

Table 6 details numerical values for EW corrections, integrated in the range $80 < m_{ee} < 100$ GeV and $89 < m_{ee} < 93$ GeV. Numbers for calculating EW weight using $\cos\theta^*$ definition of the scattering angle are shown. In Table 25 results obtained with wt^{EW} calculated in different frames are compared. When using *Mustraal* frame or *Collins-Soper* frame instead of $\cos\theta^*$ one, the differences are at most at the 5-th digit.

In Table 24 compared are results with wt^{EW} calculated in different frames. When using *Mustraal* frame or *Collins-Soper* frame instead of $\cos\theta^*$, the differences are at most at the 5-th digit.

Table 24: EW corrections to cross-sections around Z-pole, $89 < m_{ee} < 93$ GeV. The EW weight is calculated with $\cos\theta^{*}$, $\cos\theta^{Mustraal}$ or $\cos\theta^{CS}$ definitions for scattering angle.

Corrections to cross-section ($89 < m_{ee} < 93$ GeV)	$wt^{EW}(\cos\theta^{*})$	$wt^{EW}(\cos\theta^{Mustraal})$	$wt^{EW}(\cos\theta^{CS})$
σ(EW corr. to m_W)/σ(EW LO $\alpha(0)$)	0.97114	0.97115	0.97114
σ(EW corr. to $\chi(Z),\chi(\gamma)$)/σ(EW LO $\alpha(0)$)	0.98246	0.98247	0.98246
σ(EW/QCD FF no boxes)/σ(EW LO $\alpha(0)$)	0.96469	0.96471	0.96470
σ(EW/QCD FF with boxes)/σ(EW LO $\alpha(0)$)	0.96473	0.96475	0.96474
σ(*LEP*)/σ(EW/QCD FF with boxes)	1.01102	1.01103	1.01102
σ(*LEP with improved norm.*)/σ(EW/QCD FF with boxes)	1.00100	1.00102	1.00100

Table 25: The difference in forward-backward asymmetry, ΔA_{FB} around Z-pole, m_{ee} = 89 - 93 GeV. The difference is calculated using $\cos\theta^{CS}$ to define forward and backward hemisphere. The EW weight is calculated with $\cos\theta^{*}$, $\cos\theta^{Mustraal}$ or $\cos^{CS}$.
Numbers should be updated with Dizet 6.XX form factors.

Corrections to A_{FB} ($89 < m_{ee} < 93$ GeV)	$wt^{EW}(\cos\theta^{*})$	$wt^{EW}(\cos\theta^{ML})$	$wt^{EW}(\cos\theta^{CS})$
A_{FB}(EW/QCD corr. to m_W) - A_{FB}(EW LO $\alpha(0)$)	-0.02097	-0.02112	-0.02101
A_{FB}(EW/QCD corr. to $\chi(Z),\chi(\gamma)$) - A_{FB}(EW LO $\alpha(0)$)	-0.02066	-0.02081	-0.02070
A_{FB}(EW/QCD FF no boxes) - A_{FB}(EW LO $\alpha(0)$)	-0.03535	-0.03560	-0.03542
A_{FB}(EW/QCD FF with boxes) - A_{FB}(EW LO $\alpha(0)$)	-0.03534	-0.03559	-0.03541
A_{FB}(*LEP*) - A_{FB}(EW/QCD FF with boxes)	-0.00006	-0.00005	-0.00006
A_{FB}(*LEP with improved norm.*) - A_{FB}(EW/QCD FF with boxes)	-0.00005	-0.00005	-0.00005

F Powheg_ew

Comments:
This text should be completed by the authors, for now as placeholders some tables from past meetings.
Recently presented materials:
`https://indico.cern.ch/event/829225/contributions/3481094/attachments/1871705/3080271/piccinini.pdf`

F.1 Benchmark results for different EW schemes

Comments:
Those tables should be completed by the authors, for now as placeholders.
Recently presented materials:
`https://indico.cern.ch/event/829225/contributions/3481094/attachments/1871705/3080271/piccinini.pdf`

Tables:

- Table 26: Cross-section and cross-section ratios at EW LO, NLO, NLO+HO, different EW schemes, `Powheg_ew` Monte Carlo. *Status of December 2018.*
- Table 27: Cross-sections, cross-sections difference in forward and backward hemispheres and forward-backward asymmetry, `Powheg_ew` Monte Carlo, EW LO, NLO, NLO+HO, different schemes.*Status of December 2018.*
- Table 28: Forward-backward asymmetry differences between different EW schemes, as estimated by `Powheg_ew`, different EW schemes at LO, NLO, NLO+HO.*Status of December 2018.*

Table 26: Cross-sections and cross-sections ratios estimated with `Powheg_ew` for three mass windows. The pole definition is used for input parameters as in Table 14.

	EW order	m_{ee} = 89 - 93 GeV	m_{ee} = 80 - 100 GeV	m_{ee} = 70 - 120 GeV
$\alpha(0)$ v0	LO	630.848722	906.156051	959.658977
$\alpha(0)$ v1	LO	571.411296	821.363274	870.729908
G_μ	LO	612.514433	880.446121	933.363827
$\alpha(0)$ v1	NLO	600.185042	863.142557	915.580114
G_μ	NLO	607.142292	873.173294	926.253246
$\alpha(0)$ v1	NLO+HO	607.551746	873.717147	926.761229
G_μ	NLO+HO	607.515354	873.655348	926.681425
$\alpha(0)$ v1	NLO/LO	1.050350	1.05087	1.05151
G_μ	NLO/LO	0.991230	0.99174	0.99238
$\alpha(0)$ v1	NLO+HO/LO	1.063247	1.063740	1.064349
G_μ	NLO+HO/LO	0.991038	0.992287	0.992840
$\alpha(0)$ v1 / $\alpha(0)$ v0	LO	0.90578	0.906426	0.90733
G_μ / $\alpha(0)$ v1	LO	1.07193	1.07193	1.07193
G_μ / $\alpha(0)$ v1	NLO	1.01159	1.01162	1.01166
G_μ / $\alpha(0)$ v1	NLO+HO	0.99994	0.99993	0.99991
G_μ / $\alpha(0)$ v0	LO	0.97094	0.97163	0.97260

Table 27: Cross-sections, cross-sections difference in forward and backward hemispheres and forward-backward asymmetry as estimated by `Powheg_ew`, for three mass windows. The pole definition is used for input parameters as in Table 14.

	EW order	m_{ee} = 89 - 93 GeV	m_{ee} = 80 - 100 GeV	m_{ee} = 70 - 120 GeV
σ $\alpha(0)$ v0	LO	630.848722	906.156051	959.658977
σ $\alpha(0)$ v1	LO	571.411296	821.363274	870.729908
σ G_μ	LO	612.514433	880.446121	933.363827
Δ_{FB} σ $\alpha(0)$ v0	LO	42.2123628	57.9248406	60.0147094
Δ_{FB} σ $\alpha(0)$ v1	LO	26.5928310	35.6782853	36.6828324
Δ_{FB} σ G_μ	LO	42.2123628	57.9248406	60.0147094
A_{FB} $\alpha(0)$ v0	LO	0.06691361	0.06392369	0.06253754
A_{FB} $\alpha(0)$ v1	LO	0.04653886	0.04343789	0.04212883
A_{FB} G_μ	LO	0.04653886	0.04343789	0.04212883
σ $\alpha(0)$ v1	NLO	600.185042	863.142557	915.580114
σ G_μ	NLO	607.142292	873.173294	926.253246
Δ_{FB} σ $\alpha(0)$ v1	NLO	18.0312902	23.2253069	23.5291169
Δ_{FB} σ G_μ	NLO	17.6425904	22.6341188	22.8962216
A_{FB} $\alpha(0)$ v1	NLO	0.03004289	0.02690785	0.02569858
A_{FB} G_μ	NLO	0.02905841	0.02592168	0.02471918
ΔA_{FB} $\alpha(0)$ v1	NLO-LO	-0.0164959	-0.0165300	-0.0164302
ΔA_{FB} G_μ	NLO-LO	-0.0174805	-0.0175162	-0.0174096
σ $\alpha(0)$ v1	NLO+HO	607.551746	873.717147	926.761229
σ G_μ	NLO+HO	607.515356	873.655348	926.681425
Δ_{FB} σ $\alpha(0)$ v1	NLO+HO	18.7322427	24.2066243	24.5563891
Δ_{FB} σ G_μ	NLO+HO	18.7739638	24.2682506	24.6205407
A_{FB} $\alpha(0)$ v1	NLO+HO	0.03083234	0.02770533	0.02649700
A_{FB} G_μ	NLO+HO	0.03090286	0.02777783	0.02656851
ΔA_{FB} $\alpha(0)$ v1	NLO+HO-LO	-0.0157065	-0.0157326	-0.0156318
ΔA_{FB} G_μ	NLO+HO-LO	-0.0156360	-0.0156596	-0.0155603

Table 28: Forward-backward asymmetry differences between different EW schemes, as estimated by `Powheg_ew`, for three mass windows. The pole definition is used for input parameters as in Table 14.

ΔA_{FB}	EW order	m_{ee} = 89 - 93 GeV	m_{ee} = 80 - 100 GeV	m_{ee} = 70 - 120 GeV
$\alpha(0)$ v1 - $\alpha(0)$ v0	LO	-0.020375	-0.020486	-0.020487
G_μ - $\alpha(0)$ v0	LO	-0.020375	-0.020486	-0.0204871
G_μ - $\alpha(0)$ v1	LO	0.0	0.0	0.0
G_μ - $\alpha(0)$ v1	NLO	-0.00098	-0.00098	-0.00098
G_μ - $\alpha(0)$ v1	NLO + HO	-0.00007	-0.00007	-0.00007

G MCSANC

Comments:
This text should be completed by the authors, for now as placeholders some tables from past meetings.
Recently presented materials:

G.1 Benchmark results for different EW schemes

Table 29: Cross-sections and cross-sections ratios estimated with MCSANC for three mass windows. The pole mass definition is used for input parameters as in Table 14.
Numbers updated on 16.10.2019 to configuration of that Table.

σ [pb]	EW order	m_{ee} = 89 - 93 GeV	m_{ee} = 80 - 100 GeV	m_{ee} = 70 - 120 GeV
$\alpha(0)$ v1	LO	571.41(1)	821.36(1)	870.72(1)
G_μ	LO	612.53(1)	880.47(1)	933.39(1)
$\alpha(0)$ v1	NLO	600.08(1)	863.00(1)	915.42(1)
G_μ	NLO	607.41(1)	873.57(1)	926.66(1)
$\alpha(0)$ v1	NLO+HO			
G_μ	NLO+HO			
$\alpha(0)$ v1	NLO/LO	1.05017	1.05070	1.05134
G_μ	NLO/LO	0.991641	0.992163	0.992790
$\alpha(0)$ v1	NLO+HO/LO			
G_μ	NLO+HO/LO			
G_μ / $\alpha(0)$ v1	LO	1.071962	1.071966	1.071975
G_μ / $\alpha(0)$ v1	NLO	1.012215	1.012245	1.012278
G_μ / $\alpha(0)$ v1	NLO+HO			

Table 30: Forward-backward asymmetry and differences estimated with MCSANC for three mass windows. The pole mass definition is used for input parameters as in Table 14.
Numbers updated on 16.10.2019 to configuration of that Table.

A_{FB}	EW order	m_{ee} = 89 - 93 GeV	m_{ee} = 80 - 100 GeV	m_{ee} = 70 - 120 GeV
$\alpha(0)$ v1	LO	0.004655(1)	0.004347(1)	0.004215(1)
G_μ	LO	0.004656(1)	0.004347(1)	0.004215(1)
$\alpha(0)$ v1	NLO	0.003058(1)	0.002746(1)	0.002623(1)
G_μ	NLO	0.002964(1)	0.002652(1)	0.002530(1)
$\alpha(0)$ v1	NLO+HO			
G_μ	NLO+HO			
$\alpha(0)$ v1	NLO - LO	-0.001597(1)	-0.001601(1)	-0.001591(1)
G_μ	NLO - LO	-0.001691(1)	-0.001695(1)	-0.001685(1)
$\alpha(0)$ v1	NLO+HO - LO			
G_μ	NLO+HO - LO			
G_μ - $\alpha(0)$ v1	LO	0.0	0.0	0.0
G_μ - $\alpha(0)$ v1	NLO	0.000094	0.000094	0.000093
G_μ - $\alpha(0)$ v1	NLO+HO			

H KKMC_hh

Comments:
This text should be completed by the authors

I HORACE

Comments:
This text should be completed by the authors